This is a preprint, the final version is subject to change, of the American Mineralogist (MSA)
Cite as Authors (Year) Title. American Mineralogist, in press.
DOI: https://doi.org/10.2138/am-2018-6370

REVISION 3

(REFERENCE FORMATS FIXED)

(IMPLICATIONS SECTION REVISED per REQUEST BY EDITOR)

Towards the wider application of ^{29}Si NMR spectroscopy to paramagnetic transition metal silicate minerals and glasses, 2: Fe(II), Co(II), and Ni(II) silicates

Jonathan F. Stebbins*
Dept. of Geological Sciences, Stanford University, Stanford CA 94305 USA

Ryan J. McCarty
Dept. of Geological Sciences, Stanford University, Stanford CA 94305 USA

Aaron C. Palke
Gemological Institute of America, 5355 Armada Drive, Carlsbad CA 92008 USA

*E-mail: stebbins@stanford.edu

submitted to American Mineralogist
revised version 1/30/2018

This is a preprint, the final version is subject to change, of the American Mineralogist (MSA)
Cite as Authors (Year) Title. American Mineralogist, in press.
DOI: https://doi.org/10.2138/am-2018-6370

Abstract

In studies of the structures of silicate minerals and glasses, ^{29}Si NMR spectroscopy has been applied almost exclusively to materials containing relatively low concentrations of ions with unpaired electrons spins, such as most transition metals and rare earths, because of sometimes severe broadening and shifting of resonances in such strongly paramagnetic systems. However, by adapting experimental methods to allow detection of very broad signals, and by examining a much expanded range of frequencies, we show here that accurate spectra can indeed be measured for a series of pure-phase transition metal silicates, including olivines (Fe_2SiO_4, Co_2SiO_4, Ni_2SiO_4), Co-akermanite ($CoCa_2Si_2O_7$), and clinopyroxenes ($CoCaSi_2O_6$, $NiCaSi_2O_6$). For the latter two, we also present data for glasses of the same nominal compositions. For all of these phases, NMR peak broadening is large, in many cases to the point where magic-angle spinning (MAS) does not enhance resolution; in all cases the observed paramagnetic shifts fall far outside the known range for diamagnetic silicates. There are clearly large effects of local structure on shift, suggesting great potential sensitivity to variations in chemical, electronic and magnetic structure in both crystalline and amorphous phases. In particular, the spectra for the glasses are very different from those of crystals in both width and position. In most cases, measured spin-spin relaxation times are long enough to avoid major loss of signal during the NMR acquisition, but this may not always be the case in more magnetically dilute solid solutions, where small, broad paramagnetic resonances due to first cation neighbor interactions may in some systems be difficult to detect. To explore this issue, we present new data on a Ni-doped forsterite ($Mg_{1.9}Ni_{0.1}SiO_4$) and on natural San Carlos olivine ($Mg_{1.8}Fe_{0.2}SiO_4$), which improve upon the accuracy of our previous studies of these materials. It is clear that applications of NMR to paramagnetic silicates holds great promise not only for empirical studies of structure

of a much wider range of compositions of minerals and glasses, but for future testing and application of advanced theoretical methods to more completely interpret such results.

Introduction

^{29}Si NMR spectroscopy has been widely applied to crystalline and glassy silicates for decades, most commonly with resolution greatly enhanced by magic angle sample spinning (MAS) methods (Engelhardt and Michel, 1987; Kirkpatrick, 1988; MacKenzie and Smith, 2002; Stebbins and Xue, 2014). However, nearly all such studies have been of materials with low (less than a few %) contents of cations with unpaired electron spins, such as most transition metal and rare earth ions, because these can interact strongly with the observed nuclear spins, often leading to severe broadening of spectra even to the point of apparent loss of signal (Grimmer et al., 1983; Hartman et al., 2007; Sherriff and Hartman, 1985). This poses an unfortunate gap in our tools to investigate questions of short-range structure and order/disorder, given the wide importance of transition metal, rare earth, and actinide-rich silicates in the earth sciences and for technology.

Some initial steps have been made in closing this gap by the discovery and quantitation of well-resolved, usually small, ^{29}Si (and ^{27}Al) NMR resonances that are displaced well away from typical chemical shifts by relatively low concentrations (ca. 0.1 to 20%) of cations such as Fe^{2+}, Co^{2+}, and Ni^{2+} in garnets, olivines, zircons and other minerals (Begaudeau et al., 2012; Dajda et al., 2003; McCarty et al., 2015; Palke and Stebbins, 2011b; Palke et al., 2015; Stebbins and Kelsey, 2009; Stebbins et al., 2017); analogous observations have been long been known for ^{89}Y and ^{119}Sn NMR spectra of rare-earth stannate pyrochlores (Grey et al., 1989; Grey et al., 1990) and have been reported recently for ^{17}O in MgO and CaO (McCarty and Stebbins, 2016b), ^{27}Al in aluminate garnets (YAG) (George et al., 2013; McCarty and Stebbins, 2016a) and ^{31}P in

REE-doped monazites ($LaPO_4$) and xenotimes (YPO_4) (Palke and Stebbins, 2011a; Palke et al., 2013). However, a key part of understanding the complex physics behind such "paramagnetic shifts" must be their measurement in pure-phase end member compounds (e.g. transition metal silicates), where site occupancies, ordering, and short-range structure are well known, reducing possible ambiguities in data interpretation. Very few such studies have been published, in part because of significant challenges in even recording such spectra accurately (Saji et al., 1973). We have begun to make progress in this area with an initial report on paramagnetic Cu(II) silicates (Stebbins, 2017); a very recent study on low temperature magnetic ordering in $(Ba,Sr)CuSi_2O_6$ also reported high-resolution ^{29}Si spectra (Puphal et al., 2016). In these compounds, the single unpaired electron spin on Cu^{2+} resulted in only moderate peak broadening, which allowed the detection of ^{29}Si NMR peaks that ranged from about +1600 ppm to –250 ppm, even in a single mineral with multiple Si sites; these are far outside the known range for SiO_4 groups in diamagnetic silicates (about –60 to –120 ppm).

The feasibility, and eventual structural utility, of NMR for paramagnetic silicates is strongly suggested, and inspired by, extensive recent work on NMR of ^{31}P, ^{7}Li, and other nuclides in lithium/transition metal oxides and phosphates of key importance in advanced battery technology, which has driven the development of both sophisticated NMR methods and theoretical analysis (Carlier et al., 2003; Grey and Dupré, 2004; Middlemiss et al., 2013; Pecher et al., 2017; Pigliapochi et al., 2017; Strobridge et al., 2014; Tucker et al., 2002; Wilcke et al., 2007; Yoon et al., 2004; Zeng et al., 2007). Some of the now well-studied Mn, Fe, Co, Ni phosphate materials (most notably $LiMPO_4$ olivines) have structures closely analogous to important silicate minerals. Although acquisition of ^{29}Si spectra in analogous silicate minerals is expected to be considerably more difficult because of the much lower natural abundance of this

nuclide (4.7% vs. 100% for ^{31}P), and by its lower resonant frequency at a given external magnetic field (about half that of ^{31}P, reducing NMR signal strength further), the experimental methodology, and to some extent theoretical interpretations, can be expected to be transferable. Here we report new data on pure-phase Fe, Ni, and Co silicate olivines (M_2SiO_4) and on Ni and Co clinopyroxenes having the diopside structure ($MCaSi_2O_6$), as well as glasses corresponding to the latter two compositions. We also present improved data on two relatively dilute olivine solid solutions studied previously, $Mg_{1.9}Ni_{0.1}SiO_4$ (5% Ni forsterite) and natural San Carlos olivine ($Mg_{1.8}Fe_{0.2}SiO_4$) (McCarty et al., 2015), to allow better connections between data for pure-phase and dilute paramagnetic minerals.

Paramagnetic shifts in solid-state NMR spectra

The physics of interactions between unpaired electron and nuclear spins is complex and in many systems remains incompletely characterized. In-depth discussions of theoretical and experimental considerations have been reported, often in the context of lithium/transition metal phosphates and oxides (Grey and Dupré, 2004; Pecher et al., 2017; Pigliapochi et al., 2017); and are summarized in the mineralogical context (Palke and Stebbins, 2011a; Stebbins et al., 2017; Stebbins and Xue, 2014). In brief, two general types of interactions can cause shifts in resonant frequencies (peak positions in spectra) away from those in diamagnetic materials. The first of these, which probably is predominant in the systems studied here, is the Fermi contact shift, sometimes referred to as “transferred hyperfine coupling”. This effect essentially involves the through-bond transfer of unpaired electron spin density from a paramagnetic cation to the NMR-observed nucleus. As such, the magnitude and even the sign of the shift depend strongly on the extent and nature of orbital overlap, covalency, bond distances and angles. Such shifts can thus

be very sensitive to short-range structure and potentially informative when structural details (e.g. order/disorder) are unknown, but can be correspondingly challenging to calculate from theory. Impressive progress in this problem has been presented recently, particularly for Li battery materials (Clément et al., 2012; Middlemiss et al., 2013; Pigliapochi et al., 2017), offering promise for future results on silicates. Paramagnetic shifts for ^{31}P in such materials can be positive or negative, and can be very large, up to 1000's of ppm and contrasting with a range for this nuclide of less than 100 ppm in diamagnetic phosphates (Wilcke et al., 2007). A second kind of interaction in such systems is called the pseudo-contact shift, and involves a through-space magnetic dipolar coupling between a nuclear spin and unpaired electron spins in asymmetric sites, and is sometimes described as "classical" in the sense of not depending on a detailed quantum-mechanical description of electronic structure. This kind of coupling is generally less than that for Fermi contact shifts, but can clearly be important, even predominant, in some relatively ionic oxide materials (Grey et al., 1990).

NMR resonances with large paramagnetic shifts can be missed in conventional spectra unless specific issues are addressed in experimental parameters, such as the transmitter central frequency and bandwidth, instrumental deadtime, and data processing. More problematically, such resonances are likely to be broadened by strong couplings to unpaired electron spins. In many cases, this line broadening is severe enough so that MAS does not significantly narrow the resonance, although this technology is advancing to allow faster and faster spinning, albeit on smaller and smaller samples. Small, structurally interesting differences in the peak position (chemical shift) can be obscured, and the total NMR signal will be spread out in frequency, greatly reducing obtainable signal-to-noise ratios. In other cases broadening may be so severe that the resonance becomes effectively unobservable. However, even in the latter scenario, the

effects of the paramagnetic cations can, in principle, be detected by calibrating total observed NMR signal intensities relative to a diamagnetic standard. In this report, we encounter all of these pragmatic issues, and give some examples of how they can be characterized and how they affect analyses of results.

Samples and experimental methods

Samples

General procedures. Dried, reagent-grade starting materials were used throughout. These were thoroughly mixed by hand grinding in agate mortars; solid state reactions (excepting that for fayalite) were carried out with powders pressed into pellets using a steel die and hydraulic press. Except for the fayalite, mineral and glass syntheses were done in air in Pt crucibles or tubes. Electron microprobe data were collected with a JEOL JXA-8230 instrument, with Ni_2Si (Ni), Fe metal (Fe), Co metal or Co_2SiO_4 (Co), and diopside (Ca, Si, Mg) standards, with a 3 μm beam diameter and 2 minute counting times.

Olivine solid solutions. The San Carlos olivine (Stanford University Research Mineral Collection) sample comprised several gem-quality crystals crushed to a powder for MAS NMR (McCarty et al., 2015). The solid-state synthesis and characterization of a 5% Ni-doped synthetic forsterite ($Mg_{1.9}Ni_{0.1}SiO_4$) was also described previously (McCarty et al., 2015).

Fayalite (Fe_2SiO_4). Fayalite was synthesized by reaction of powdered Fe metal and quartz at 1070 ˚C in a CO/CO_2 gas mixing furnace, with a total reaction time of about 100 h and 4 intermediate grinding steps. A small fraction (ca. 5%) of excess silica was added to ensure complete reaction of the Fe metal. XRD data showed the presence of only fayalite and a minor

amount of excess cristobalite. The resulting powder was uniformly light greenish brown in color; EPMA detected only fayalite and a silica phase.

Co-olivine (Co_2SiO_4). Co_2SiO_4 was synthesized from Co_3O_4 (known to decompose to CoO above about 900 ˚C) and amorphous silica, heated at 1200 ˚C for a total of 57 h with one intermediate grinding step. This relatively low temperature was chosen to avoid any melting (O'Neill, 1987; Sugawara and Akaogi, 2003). A fine-grained, uniformly violet-pink sample resulted. EPMA confirmed the sample purity and stoichiometry, detecting 1-2 % only of unreacted silica.

Ni-olivine (Ni_2SiO_4). Ni_2SiO_4 was synthesized from NiO and amorphous silica, heated for a total of 240 h at 1400 ˚C with two intermediate grindings (Sugawara and Akaogi, 2003). A fine grained, uniformly pistachio-green product was the result. EPMA confirmed the stoichiometry of the olivine, with small amounts of unreacted starting materials.

$NiCaSi_2O_6$. Crystalline $NiCaSi_2O_6$ (diopside structure, (Ghose et al., 1987)) was synthesized from NiO, $CaCO_3$ and amorphous SiO_2, heated for a total of 96 h at 1300 ˚C with one intermediate grinding, yielding a homogeneous medium-green product (Durand et al., 1996; Navrotsky and Coons, 1976; Raudsepp et al., 1990). EPMA confirmed the stoichiometry of the main phase but detected a few % unreacted NiO and an unidentified low-Ni phase. The same starting mix was melted for about 1 h in a Pt tube in air for about 1 h. The resulting dark reddish-brown glass contained a few spherules of bright green NiO crystals; fragments without visible crystals were hand-picked for NMR. EPMA data showed that this glass and its Co equivalent (below) were homogeneous, and were close to the corresponding crystals in composition with 1 to 2 mole % lower NiO or CoO, probably through loss to the Pt containers during melting.

$CoCaSi_2O_6$. The starting mixture of Co_3O_4, $CaCO_3$ and amorphous silica was first melted to a homogeneous, very dark blue glass at 1300 ˚C. Part of this was crystallized at 1140 ˚C for 8 h. A second sample of crystalline $CoCaSi_2O_6$ (also diopside structure) was made by sintering the same oxide mix at 1125 ˚C for a total of 192 h with two intermediate grinding steps (Navrotsky and Coons, 1976). EPMA detected only stoichiometric $CoCaSi_2O_6$ in this product. Both crystalline samples were pink in color, with a small percentage of dark blue grains, presumably Co-akermanite. NMR data on the two crystalline samples were similar; those shown here are for the sintered sample.

Co-akermanite ($CoCa_2Si_2O_7$). Crystalline $CoCa_2Si_2O_7$ (akermanite structure, (Kusaka et al., 2001)) was synthesized from the same reagents as $CoCaSi_2O_6$, ground, pelletized, and heated for a total of 84 h at 1190 ˚C with two intermediate grindings. The product was a uniform, dark blue color. EPMA detected only the desired phase and confirmed its composition.

NMR data collection and analysis

NMR methods used here are similar to those recently described for paramagnetic Cu(II) silicates, which required exploration of large ranges in frequency of NMR signals, far beyond those for diamagnetic silicates (Stebbins, 2017), as well as methods to allow accurate observations of often very broad signals. Data were acquired with a Varian 400 MHz spectrometer (9.4 Tesla magnet, 79.5 MHz for ^{29}Si), with 3.2 mm diameter MAS rotors, and either non-spinning (“static”) samples or spinning frequencies of 10 to 22 kHz. Tetramethyl silane (TMS) at 0 ppm was the frequency reference; a natural sample of pure diopside ($CaMgSi_2O_6$) from Wakefield, Quebec was used as an intensity standard. All spectra shown here (MAS and static) were collected with a standard spin-echo pulse sequence (90°- τ - 180°) with

echo delay time τ (chosen as an integral number of rotor periods for the MAS spectra) usually of 100 μs but ranging from 60 to 900 μs in experiments to estimate spin-spin relaxation times (T_2) via the decay in signal with τ. The spin-echo method shifts the recorded time-domain signal away from residual NMR probe "ringing" and allows more accurate measurement of very broad lines, whose signals decay rapidly. For many of the samples studied here, standard 1-pulse methods, with typical instrumental deadtimes of 10's of μs, miss most or even all of the NMR signal because of this decay. However, the relatively long NMR pulses used here (typically 2.5 and 5 μs) resulted in a relatively narrow excitation bandwidth (empirically estimated as roughly 150 kHz or 1800 ppm), requiring in most cases the acquisition of several spectra with different settings of the transmitter frequency (re-tuning the NMR probe at each step), with offsets chosen as 100 kHz. These were summed to obtain the final spectra. (Such "spin-echo mapping" methods have often been applied to observe very NMR broad spectra for paramagnetic systems, for example for ^{31}P NMR of phosphate sorbed onto, and ^{27}Al of alumina dissolved into, iron oxyhydroxides (Kim et al., 2015; Kim et al., 2011), as well as pure-phase Fe(III) phosphates (Kim et al., 2010)). In addition, the very large paramagnetic shifts of some of the materials studied here (1000's of ppm) required preliminary experiments, shifting the transmitter over a wide range, to initially locate the resonances. Tests of varying times between pulse trains indicated that all spectra were fully relaxed at the 0.1 s delay generally used; in contrast the pure diopside intensity standard was run with a 1 h pulse delay to allow full relaxation and quantitative signal intensity. For the spectra shown for the Fe, Ni, Co silicates, 200,000 to 500,000 acquisitions were collected for each transmitter setting, requiring several days for each full data set. Spectral widths of 2 MHz were used; the time-domain data were processed from the top of the echo, set at a fixed time for all comparable experiments. Gaussian apodization was

chosen to enhance signal-to-noise without significantly broadening spectra (<5% of linewidth). Spin echo acquisition yielded visibly flat baselines without the need for back-predicting the FID or large first-order phase corrections, procedures which are often required in single-pulse data sets to compensate for instrumental deadtime and which can introduce distortions in line shapes. Nonetheless, minor uncertainties in baselines of the very broad spectra contributed roughly a 10 % uncertainty in estimated peak areas.

In the MAS spectra, air friction caused temperature increases of a few 10's of ˚C; because these can strongly affect positions of paramagnetically shifted peaks they were calibrated using the ^{207}Pb NMR peak shift in $Pb(NO_3)_2$ (Takahashi et al., 1999).

Areas of the composite, summed spectra were determined by integrating in non-overlapping 100 kHz windows for the component spectrum centered at each transmitter frequency; center frequencies reported here for the very broad static spectra are taken as the centers of gravity of the summed line shapes, based on the centers of their overall integrals. Reported areas are normalized per mg of SiO_2 in the sample in the probe, for comparison among samples and with the diopside standard.

Results

MAS spectra for pure-phase crystals

The crystalline, pure-phase Ni silicates showed the smallest amount of broadening in both static and MAS ^{29}Si spectra, probably at least in part because Ni^{2+} has only 2 unpaired electron spins per cation, compared with 3 for Co^{2+} and 4 for Fe^{2+} (assuming the normal high-spin states of low-pressure silicates). For MAS data collected with samples spinning at frequencies up to 22 kHz, full separation of spinning sidebands was observed for Ni_2SiO_4 (Fig.

1), and nearly full separation for $NiCaSi_2O6$ (Fig. 2). Even in the most-resolved spectrum, however, the widths of the individual central peak and sidebands were much greater than in typical, ordered, diamagnetic silicates (ca. 100 ppm full width at half maximum, FWHM, for $NiCaSi_2O_6$, 20 ppm for Ni_2SiO_4 vs. ca. 0.2 ppm for pure Mg_2SiO_4). Much less effective narrowing by MAS, and only partial resolution, was seen for Co-silicates (Fig. 2), and very little narrowing for pure-phase Fe_2SiO_4. For the Ni-silicates, MAS sideband (ssb) patterns roughly mapped out the observed static (non-spinning, see below) line shapes (Fig. 1), but the sideband manifold was typically somewhat narrower than that of the static peak, probably because of excitation bandwidth limitations: the MAS spectra were generally collected with data from only a single transmitter frequency. For all of the pure-phase transition metal silicates studied here, peak positions are shifted far outside of the known range for SiO_4 groups in diamagnetic silicates (about –60 to –120 ppm), either to higher or to lower frequencies.

As is often the case with spectra containing large number of sidebands (i.e. the spinning frequency is much lower than the total static linewidth), the most intense peak does not necessarily correspond to the isotropic chemical shift δ_{iso}, which can be somewhat difficult to identify in such cases. Typically, spectra collected with different spinning rates can be compared to find the position of the peak that is independent of the rate, which can then be identified as δ_{iso}. However, paramagnetic shifts are often strongly temperature dependent, and sample heating (up to a few 10's of ˚C) caused by air friction on the sample rotor can cause spin-rate dependent changes in peak positions (McCarty et al., 2015; Palke and Stebbins, 2011a; Palke and Stebbins, 2011b; Stebbins, 2017): in general, the magnitudes of paramagnetic shifts become smaller at higher temperatures as the Boltzmann distribution of low and high energy states for the unpaired electrons approaches unity (Palke and Stebbins, 2011a; Wilcke et al., 2007). This effect can be

clearly seen in data for Ni_2SiO_4. Figure 3 shows expanded views of the central regions of spectra collected at a wide range of spinning rates, with mean rotor temperatures. We thus identify the peak near to –810 ppm in the near room temperature spectrum as the likely 'central' peak representing δ_{iso}. An isotropic average shift near to –810 ppm is also most consistent with the center of gravity of the static spectrum of –820 ± 20 ppm (see below). The increase in width and the development of a complex peak shape in the higher spinning speed data are probably caused by the growth with spinning rate of significant temperature gradients in the sample rotor, as was reported recently for Cu(II) silicates (Stebbins, 2017).

The minor amount of unreacted silica known to be present in this sample (see experimental section) was not detected by the NMR, presumably because of a much longer spin-lattice relaxation time, as expected for a nearly pure cristobalite vs. a phase rich in paramagnetic cations. This same finding applied to the fayalite sample (below).

Static (non-MAS) spectra

Because of the lack of full (or in some cases, of any) line narrowing by 20 to 22 kHz MAS for most of the materials studied here, static (non-MAS, stationary samples) spectra were collected. For all of the samples, however, static peak widths were broad enough so that spectra collected at a fixed radiofrequency transmitter setting recorded only part of the line shape, due to the relatively narrow excitation bandwidth of the echo pulses used to record the spectra (roughly 150 kHz or about 1800 ppm for ^{29}Si). This was a minor issue for the narrowest spectra (for Ni_2SiO_4 and $NiCaSi_2O_6$), but of major importance for the other crystalline silicates and especially for the glasses. As has been well-established in other 'wideline' spectra of paramagnetic materials (Kim et al., 2015; Kim et al., 2011; Kim et al., 2010) (and other systems

with extremely broad NMR lines), this problem was overcome here by the relatively time-consuming approach of systematically changing the spectrometer frequency (here, in 100 kHz ≈ 1260 ppm increments) and recording a series of spectra that were summed to give a composite spectrum that accurately represented the full static line shape. A typical example is shown for Co_2SiO_4 in Fig. 4.

Static spectra for Fe_2SiO_4, Co_2SiO_4, and Ni_2SiO_4 are compared in Fig. 4; data for the mean isotropic shifts and widths are in Table 1. Data for the Co-olivine can be compared to a single previous report of an imprecisely measured room temperature shift of "0.03±0.02 %" relative to a glass sample tube (Saji et al., 1973). Adjusting to modern units and standard, this would be roughly 200 ± 200 ppm relative to TMS, but the early study was primarily focused on low-temperature magnetic ordering in the olivine and did not actually show any spectra. Our new data show that shifts are in fact generally large relative to those in diamagnetic silicates, as expected from our recent study of Cu(II) silicates, and, in particular, from extensive recent studies of paramagnetic shifts for ^{31}P in analogous $LiMPO_4$ (M=Mn, Fe, Co, Ni) olivine phases and related oxide and phosphate battery materials (Wilcke et al., 2007). Peak widths (Table 1) are also large, and may be dominated by the large magnetic susceptibility anisotropy expected in these minerals with relatively low symmetries, and/or large electron-nuclear dipoalr couplings. The asymmetric static line shapes, especially as seen for the clinopyroxene phases (below), are somewhat analogous to 'powder patterns' observed for spin 1/2 nuclides in some diamagnetic systems, which reflect anisotropy in the chemical shifts (CSA). The centers of gravity of the peaks, which represent the average over all orientations of such anisotropic effects, range widely from +3200 ppm for Fe_2SiO_4 to –820 ppm for Ni_2SiO_4.

Static spectra for crystalline (diopside structure) and glassy $NiCaSi_2O_6$ are shown in Fig. 5. The anisotropic line shape is well-developed for the crystalline sample, and is seen in both the static and MAS spectra (Fig. 2); its center of gravity (+3000 ppm) is far above that for Ni_2SiO_4 (–820 ppm). The spectrum for the glass is much broader and shifted to much lower frequency than for the crystal, probably reflecting major short-range structural differences as well as heterogeneity in medium-range distributions of paramagnetic cations in the glass (see below). A small fraction of the total observed signal for the glass is narrowed significantly by MAS, again suggesting heterogeneity, with some SiO_4 groups without nearby Ni^{2+} neighbors. The position of this component (ca. –85 ppm) is within the range for diamagnetic silicates, but its width (ca. 100 ppm) remains abnormally large: MAS linewidths for diamagnetic amorphous silicates are typically <25 ppm. This component could be inherent to the glass, or could be due to a minor crystalline impurity or even to incipient liquid-liquid phase separation, undetected by EPMA analysis and X-ray mapping. Determining its origin will be of interest in future studies.

Spectra for crystalline and glassy $CoCaSi_2O_6$, and crystalline $CoCa_2Si_2O_7$ are shown in Fig. 6. For the isostructural clinopyroxenes, the shift for the Co phase, and its line width, are considerably greater than those for the Ni phase, as was also seen for the olivines. Again, the linewidth for the glass is much greater than for the crystal, and the average peak position is shifted much less from the "normal", diamagnetic range. A minor component in the glass, as for the Ni analog, is again somewhat narrower in both the static and MAS (not shown) spectra. The akermanite phase, $CoCa_2Si_2O_7$, which has Co in tetrahedral sites instead of the octahedral sites in the clinopyroxene and olivine phases, also has a much lower shift than crystalline $CoCa_2Si_2O_7$.

Spin-echo MAS and static spectra, solid solutions

As reported previously (McCarty et al., 2015), the MAS spectrum (20 kHz spinning rate) of San Carlos olivine (ca. $Mg_{0.9}Fe_{0.1}SiO_4$) at first appears to be dominated by a broad (75 ppm FWHM) peak centered ("A" in Fig. 7) slightly above the normal range for diamagnetic silicates (–50 ± 5 ppm); this width epitomizes the loss in resolution, or even (for early NMR methods) the total loss in signal resulting from major contents of paramagnetic cations (Grimmer et al., 1983), as the spectrum for pure Mg_2SiO_4 has a line width of about 0.2 ppm. Slightly faster spinning enhances resolution further, revealing the presence of at least one additional paramagnetically shifted peak ("B" in the figure), whose isotropic position appears to be at about –200 ppm but which could actually be hidden under the shoulder of the main peak near to +70 ppm (with the –200 ppm peak a sideband). Both of these possible positions are shifted farther from the diamagnetic resonance (–61.8 ppm) than the tiny paramagnetic peaks reported for Mg_2SiO_4 (forsterite) with low (0.05 to 0.4 %) Fe_2SiO_4 component (McCarty et al., 2015), which ranged from about –26 to –101 ppm (relative shifts of about +39 ppm to –39 ppm). However, it is important to also note that when spin echo MAS spectra are collected, and combined from several frequency offsets, it can now be seen that roughly 60 to 80% of the observable ^{29}Si signal for this mineral remains in a very broad, unresolved peak (Fig. 7, 8). The latter presumably is dominated by contributions from Si sites with one or more first-neighbor Fe^{2+} cation neighbors.

The composite, static spectrum of this olivine allows further comparison with the pure-phase samples (Fig. 8). This line shape is complex, with a narrower and a broader component or possibly a range of components with varying widths. The overall peak has intensity above baseline from at least +4000 to –2000 ppm and a width (FWHM) of about 2500 ppm. A rough estimate indicates that about 65±5 % of the area of the composite static spectrum (at echo delay

373 of 100 μs) is in the broader component. The overall center of gravity of the composite static
374 spectrum is about 0±100 ppm.

375 Spin-echo MAS spectra for Mg_2SiO_4 with a 5% Ni_2SiO_4 component ($Mg_{1.9}Ni_{0.1}SiO_4$)
376 displayed the same set of small, paramagnetically shifted peaks (at about –10 to –70 ppm) as
377 described in our recent study using the more conventional single-pulse excitation (McCarty et
378 al., 2015). As shown in Figure 9, however, one additional, relatively broad resonance was also
379 detected, centered at about +135 ppm, again well outside of the range previously reported (ca.
380 50 ppm FWHM, 6±2 % of observed area for echo delays of 2 rotor periods). Spectra (both MAS
381 and static) collected with the transmitter offset up to 200 kHz above or below the main peak
382 center detected no additional resonances, either narrow or broad, at the obtainable signal to noise
383 ratio. The static spectrum (Fig. 8) is relatively narrow (FWHM=108 ppm) and featureless,
384 although slightly asymmetrical: a minor shoulder on the high frequency side may corresponds to
385 the +135 ppm shifted resonance. The overall spectrum is about twice as wide as the static
386 spectrum of pure forsterite (Stebbins et al., 2009), indicating only a relatively minor effect of the
387 paramagnetic cation on the overall line shape.
388
389 **Signal loss, spin-spin relaxation, and peak areas**
390 In simple "one pulse" NMR experiments often used to record high resolution (MAS)
391 spectra for solids, the time-domain signal (free-induction decay or FID) is recorded immediately
392 after a short instrumental dead time necessitated in part by a finite time required for the
393 excitation signal (observe pulse) to decay from the probe circuit ("probe ringing"). Typical dead
394 times of about 10 to 40 microseconds (μs) generally have no significant effect on narrow, high
395 resolution spectra, because the FID can persist for 10's to 100's of milliseconds (ms) or even

longer. However, for very broad spectra as described here, the FID may decay in 10's of μs, often making it nearly unobservable by "one pulse" methods. In such cases, the loss of signal can be detected by intensity calibration of the observed residual signal with known standards. A spin-echo pulse sequence, such as employed here, shifts the FID out in time from the end of the observation pulses, in principle allowing its accurate observation without dead time or "probe ringing" effects. However, spin-spin relaxation during the echo delay (typically 100 μs here) can lead to decay of the signal, characterized by an exponential function that can be written as $\ln(M/M_0) = -\tau/T_2$, where M is the observed signal intensity, M_0 is that at zero time (here taken as the expected value from a standard calibration), τ is the echo delay time, and T_2 is the spin-spin relaxation time, approximated here as a constant for each data set. Measurements of signal strength (peak areas in the Fourier-transformed spectra) as a function of τ thus yield estimates of T_2, as given in Table 2; representative data are plotted in Figure 10. These data can then be used to correct the observed signal intensity (obtained by integration and normalized to the mass of SiO_2 in the sample) back to zero time, and thus obtain a more accurate comparison among samples and between samples and standards.

The peak areas reported in Table 2 are the sums of the integrals of non-overlapping, 100 kHz-wide frequency windows centered at each offset of the transmitter frequency and spanning the total range of observable signals for each material. The latter was defined as data for transmitter settings that yielded signals greater than about 5 % of the total detected at all frequencies. The T_2 given for the pure-phase crystalline samples are based on data for the transmitter setting giving the most intense (or an average of the two most intense) signal. For these, measurements on the lower intensity components at different center frequencies yielded values that were similar but more uncertain.

In some reported cases, for example ^{29}Si spectra of the paramagnetic Cu(II) mineral cuprorivaite ($CaCuSi_4O_{10}$) (Stebbins, 2017), a very short T_2 (ca. 35 μs for this example) can lead to loss of much of the NMR signal during a typical spin-echo experiment. However, for the pure-phase Ni, Co, Fe silicates here, T_2 values, although ranging widely from about 500 to 4000 μs, are all long enough so that signal loss during a 100 μs echo delay is less than 20% and most commonly <10% (Table 2). Correcting the observed, integrated intensities to zero time, it can be seen that the measured values are within 5 to 10 % of those expected from data collected for a pure diopside standard with the same pulse sequence and instrumental settings (apart from a delay between pulse trains of 1 hour for the standard instead of 0.1 s for the paramagnetic samples). This is probably well within the errors associated with observing such wide and inherently noisy spectra, and suggests that this approach can indeed produce relatively accurate spectra even when overall linewidths are three or four orders of magnitude greater than those typically measured in diamagnetic samples. The data for these samples thus rule out any large spectral components that decay extremely rapidly in these samples (i.e. that are lost entirely in less than the minimum echo delays of 50 to 100 μs explored here); in turn the lack of any large "invisible" component of the NMR signal makes interpretation of data for materials with unknown structures (e.g. glasses) somewhat more straightforward.

In two of the samples (Ni_2SiO_4 and Fe_2SiO_4) known to have minor amounts of unreacted silica, NMR signals for this phase were not detected due to the long spin-lattice relaxation time of pure silica (i.e. its NMR signal presumably 'saturated' with the short pulse delays used here). Given that integrated peak areas were normalized to the total sample weights, this second phase would introduce a corresponding error, i.e. the tabulated values would be proportionally underestimated. This appears most obviously for Fe_2SiO_4.

The two olivine solid solutions (San Carlos olivine and $Mg_{1.}Ni_{0.1}SiO_4$) studied here by spin-echo and variable transmitter offset methods were both previously investigated by one-pulse NMR methods along with a series of more dilute Fe, Co, Ni olivines (McCarty et al., 2015). The new data showed somewhat more complex T_2 and peak area behavior than for the pure-phase samples. For the Ni-doped forsterite, in spite of high signal-to-noise resulting from long acquisitions at a range of transmitter settings, the only observable components of the spectrum were fully narrowed by MAS, with maximum widths of about 50 ppm. The total observed area (with echo delays of 90 to 100 μs), out to ±500 ppm from the center, is about 25 to 30 % below that expected from the pure diopside standard (Table 2). The multiple, well-resolved paramagnetically shifted peaks for this sample present an opportunity to measure T_2 values for ^{29}Si in sites with varying degrees of interaction with the unpaired electron spins on the Ni^{2+} cation(s). As shown in Figure 9, large changes in the echo time τ do indeed affect the relative peak intensities: the central peak is reduced only slightly by increasing τ, the closer-in shifted peaks more, and the newly-observed resonance at +135 ppm is reduced nearly to undetectability at the longest τ explored (909 μs). This requires systematically shorter T_2 values for resonances with larger shifts (Table 2, Figure 10). For the +135 ppm peak, extrapolation back to a zero echo delay leads to a significant increase in its estimated contribution to the total observable signal, i.e. from about 6% at τ = 91 μs to 10±2% at τ = 0. The static spectrum for this sample showed no detectable features at higher or lower frequencies than seen in the MAS spectra (Fig. 8), but its integrated intensity is significantly higher, only about 15 to 20% below the standard value.

In contrast to the Ni-doped forsterite, the MAS and static spectra for the San Carlos olivine clearly show a major, broad component that is not narrowed by MAS. This broad feature also has a relatively short T_2, about 2 times shorter than that of the overall composite spectrum

(Table 2). This can be clearly seen by comparing its relative contribution to spectra collected with short vs. long spin echo delays (Fig. 8) Correction back to a zero echo delay indicates that most of the signal for this sample is detectable (Table 2).

The data for the $CoCaSi_2O_6$ glass also show faster spin-spin relaxation for the most shifted (highest frequency) components, with T_2 estimated as low as about 500 μs, in contrast to the average for the entire spectrum of about 1800 μs (Table 2). However, given the relatively low obtainable signal to noise ratio, correction to zero echo delay for all components does not yield a line shape very different from that shown in Figure 6.

Discussion

Paramagnetic shifts and short-range crystal structure

Analysis of paramagnetic shifts of NMR resonances in oxide and silicate materials remains a challenging problem, as the physics of the underlying interactions between unpaired electron and nuclear spins is complex and quantitative theoretical predictions remain difficult. The first detailed studies of any such spectra in silicates with major, stoichiometric components of magnetic transition metal cations (Cu(II) silicates) have been reported only recently and probably raised more questions than answered, apart from clearly showing that collecting such data is feasible and potentially that they can carry structurally important information (Stebbins, 2017). Another very recent study of low temperature magnetic transitions in $Sr_xBa_{1-x}CuSi_2O_6$ solid solutions also presented room-temperature ^{29}Si MAS spectra with paramagnetic shifts of up to 500 ppm (0.05%), although the frequency reference was not reported (Puphal et al., 2016). A number of studies of ^{29}Si spectra of minerals with relatively dilute paramagnetic components (up to a few to 20 %) do provide some initial guidance (McCarty et al., 2015; Palke and Stebbins,

2011b; Palke et al., 2015; Stebbins and Kelsey, 2009), as well, although the relatively narrow, highly-resolved spectra obtainable in such systems are quite different from the "wideline" data reported here.

Fortunately, there has been extensive work on ^{31}P (and ^{7}Li) NMR spectra of paramagnetic transition metal phosphates and oxides, in large part because of their wide and important utility in lithium ion batteries (Grey and Dupré, 2004; Pecher et al., 2017) and the critical role played by solid solutions and short-range order/disorder in the performance of such materials. Increasingly sophisticated experimental data have also driven advanced theoretical work, which has led to considerable insight into relationships between short-range crystal structure and spectra that have been important in understanding results for complex solid solutions (Yoon et al., 2004; Zeng et al., 2007). Of particular interest here are a number of studies of the $LiMPO_4$ phases (M= Mn^{2+}, Fe^{2+}, Co^{2+}, Ni^{2+}), which have the olivine structure, with octahedrally coordinated Li^{+} in the M1 site, octahedrally coordinated M^{2+} in M2, and P^{5+} in the tetrahedral sites (Abrahams and Easson, 1993). For example, fast MAS at a relatively low magnetic field of 1.5 T yielded well-resolved ^{31}P and ^{7}Li spectra, the former with paramagnetic shifts of up to 1000's of ppm (all positive) (Wilcke et al., 2007). The large magnitudes of these shifts, together with theoretical calculations (Kim et al., 2010; Middlemiss et al., 2013; Strobridge et al., 2014) have strongly suggested that they are dominated by through-bond transfer of unpaired electron spin density from the paramagnetic cation to the observed NMR nucleus (transferred hyperfine coupling or Fermi contact shift). The extent of this transfer, and the resulting effect on the frequency (paramagnetic shift) of the NMR resonance, depends strongly on the magnetic susceptibility and thus on the number of unpaired spins and their interactions if any, but also is fundamentally controlled by the covalency and orbital overlap of

511 the bonds through which the spin density is transferred. Thus, paramagnetic shifts for ^{7}Li in these
512 phases are typically only a few percent of the ^{31}P shifts, due in large part to the higher covalency
513 of the P–O bond relative to the Li–O bond (Wilcke et al., 2007). Other effects of unpaired
514 electron spins, notably through-space dipolar coupling or the "pseudocontact" shift, appear to be
515 of lesser importance in these materials.

516 For the $LiMPO_4$ olivines, a strong, systematic increase in paramagnetic shift with the
517 number of unpaired electron spins (5 for Mn^{2+}, 4 for Fe^{2+}, 3 for Co^{2+}, 2 for Ni^{2+}) was observed,
518 which was linear when corrected to temperature-independent values using systematic data on
519 variation with temperature (Wilcke et al., 2007). Room temperature values from that study are
520 shown for the Fe, Co, and Ni phosphates in Figure 11. Our new results for the silicate olivines
521 also show a systematic, roughly linear trend on the same plot, but with a much steeper slope
522 presumably related to the greater number of paramagnetic cations per tetrahedral cation in the
523 silicate structure, as well as to other structural differences and variations in coupling for the two
524 different nuclides. Our two data points for the Co,Ni clinopyroxenes ($MCaSi_2O_6$) show a trend
525 parallel to that for the silicate olivines but displaced to much higher, more positive shift values.

526 As noted above, detailed theoretical understanding of such observed contact shifts is
527 challenging, but a great deal of progress with DFT-based methods has been reported recently for
528 the phosphate olivines and related oxide materials (Clément et al., 2012; Middlemiss et al., 2013;
529 Pigliapochi et al., 2017). Here, the basic approach has involved identifying all of the first cation
530 neighbor bond paths in the structure (e.g. M–O–P), then performing a high-level calculation of
531 the electron distribution for the path, in this case focusing on the redistribution of unpaired
532 electron spin density from the transition metal 3d orbitals to the 1s orbitals of the phosphorus
533 cation, which in turn interact with the nuclear spin. The overall paramagnetic shift observed in

534 the NMR spectrum can then be approximated as the sum over all the first neighbor bond paths.
535 Because of large variation in the electronic structure (e.g. orbital overlap) for different paths, the
536 calculated individual contributions can vary widely. Values depend strongly on structural details
537 and on the approximations made in the calculation, but tend to be most different for bond paths
538 with relatively narrow M–O–P angles (ca. 90˚) common for edge-shared polyhedra vs. those for
539 more open M–O–P angles (ca. 130˚) for corner-shared connections, for example from about –
540 400 ppm for the former and about +700 for the latter in $LiCoPO_4$ (Middlemiss et al., 2013).
541 Such calculations have not yet been made for silicates, but systematic trends in the data
542 and analogy to the phosphate olivines may provide important clues as to their structural origins
543 that could be the basis for beginning to think about results for unknown structures such as
544 glasses. Apart from the large effect of numbers of unpaired electrons noted above, the most
545 striking finding is the much larger shifts for the clinopyroxenes relative to those of the silicate
546 olivines for a given M cation, a difference of almost 4000 ppm for both the Ni and Co phases.
547 This is clearly not the result of simply the number of paramagnetic cation first neighbors or to
548 the number of first neighbor M–O–Si bond pathways, which are both much greater in the
549 olivines than in the clinopyroxenes (Table 1). However, theoretical studies of the phosphate
550 olivines, and their measured paramagnetic shifts, may provide a start in accounting for such
551 dramatic structural differences. Apart from stoichiometry and number of paramagnetic M
552 neighbors per Si, the most important differences in the short-range clinopyroxene vs. olivine
553 structures (Figure 12) may be that for the former, all of the M–O–Si connections (3 per Si)
554 involve octahedral-tetrahedral corner sharing, with bond angles typically about 120 to 150˚ and
555 relatively long M–O–Si distances of about 0.32 to 0.35 nm (Durand et al., 1996; Ghose et al.,
556 1987; Raudsepp et al., 1990). In contrast, for the silicate olivines there are 9 first neighbor M

cations for each Si. Six of these form corner-shared M–O–Si linkages with bond angles typically in the range of 120 to 124˚ and M-Si distances of about 0.32 to 0.35 nm (Smyth, 1975; Tamada et al., 1983); the other three cations are in edge-shared geometries and thus form 6 M–O–Si bond paths (two each) with much narrower angles (ca. 90˚) and shorter M-Si distances (about 0.27 to 0.29 nm).

As a zero-order starting point for thinking about the paramagnetic shifts in the silicates, one could hypothesize that in the clinopyroxene structures each of the three corner-shared bond paths provides a large, positive contribution to the total shifts, as suggested by the calculations for the phosphates. This could be on the order of +1000 ppm per bond path, and larger for Co^{2+} than for Ni^{2+} given the greater number of unpaired spins (and possibly even greater for Fe^{2+}, although we lack data for $FeCaSi_2O_6$). It could then be assumed that the observed shifts for the olivines result from the sum of contributions of these values for each of the 6 corner-shared M–O–Si pathways, added to 6 large and *negative* contributions from the edge-shared linkages (due to the three edge-shared octahedral M cations). This could imply a progressively greater effect of the negative shift contributions from Fe^{2+} to Co^{2+} to Ni^{2+}.

Observed shifts for the $LiMPO_4$ olivines may provide further support for the importance of this crude but large distinction between corner-shared and edge-shared bond paths, given that in these structures, the M1 site is occupied by Li^+, which of course has no unpaired electron spins. The result is that there are 4 instead of 6 corner-shared M–O–P linkages (4 cations) and only 2 edge-shared linkages (1 cation). This could substantially reduce the negative contributions to the total shift, leading to the higher overall observed values (all positive) for the phosphates relative to the silicates.

579 However, at this point of our knowledge, we cannot be at all certain that this hypothesis
580 of large positive shifts for corner-shared linkages, partly balanced by large negative shifts for
581 edge-shared linkages, is responsible for the large observed differences between the data for
582 silicate olivines and clinopyroxenes. Other aspects of their electronic and/or magnetic structures
583 could play an important role. The olivine data, taken in isolation, could also suggest that each of
584 the nine first neighbor M cations contributes an *average* paramagnetic shift estimated as the
585 observed total simply divided by 9, yielding values of +356, +82, and –91 ppm/cation for
586 Fe_2SiO_4, Co_2SiO_4, and Ni_2SiO_4, respectively.
587 The coordination number of the paramagnetic cation itself is of course likely to also be
588 important for its contribution to NMR shifts, but this issue has rarely been explored either
589 empirically or theoretically. One result that bears on this question is the measured shift for
590 akermanite-structured $CoCa_2Si_2O_7$ (Kusaka et al., 2001), in which Co^{2+} is four-coordinated
591 instead of six-coordinated as in the olivines and clinopyroxenes. In the akermanite structure,
592 each Si has only two Co neighbors, with corner-shared Co–O–Si linkages. The observed shift of
593 +1380 is again relatively large and positive, but is lower than might be expected from the data
594 for octahedral M cation structures. This lower value comes in spite of the shorter, presumably
595 more covalent, Co–O bonds in the tetrahedra relative to octahedra, as well as shorter Co–O–Si
596 distances (ca. 0.31 nm) at similar angles (ca. 118˚). A detailed analysis of the electronic structure
597 in this phase, in particular how crystal field effects and differences in d-orbital energy levels
598 change the charge distribution around transition metal cations in octahedra vs. tetrahedral sites,
599 and how this in turn affects the Si–O bonds, would be useful for further analysis of these data,
600 which are especially interesting for results on glasses discussed below. Another comparison with
601 our results here for transition metal cations in octahedral sites in olivine and clinopyroxene are

602 several studies of the effects of Fe^{2+} in dodecahedral sites in garnets on ^{29}Si paramagnetic shifts
603 in adjacent edge-shared sites (about +200 ppm) and corner-shared sites (about –20 ppm) (Palke
604 and Stebbins, 2011b; Palke et al., 2015).
605
606 **Crystals vs. glasses**
607 The reasonably good glass-forming ability of the $NiCaSi_2O_6$ and $CoCaSi_2O_6$
608 compositions provides a nearly unique opportunity to compare ^{29}Si spectra for transition metal-
609 rich glasses and nearly-isochemical crystals. As noted above and as illustrated by Figures 5 and
610 6, in both cases the glass spectra are much (at least 2 or 3 times) wider than those for the
611 corresponding crystals, and their average paramagnetic shifts are much (2000 to 3000 ppm)
612 lower. Also as noted above, the summed, integrated peak areas for the glasses and crystals are
613 equal within about 5%, showing that the large differences in peak shapes and positions cannot be
614 due to the selective loss of a major part of the NMR signal.
615 In a very general sense, the glasses are expected to have considerable structural disorder
616 and thus a possibly wide range of SiO_4 sites with varying numbers and varying types of bond
617 pathways to first-neighbor paramagnetic cations, as well as even more disorder with respect to
618 medium- and long-range structure. Some aspects of this disorder are relatively well known from
619 spectroscopic studies of diamagnetic glass compositions, for example $MgCaSi_2O_6$ (diopside). In
620 such compositions, instead of every SiO_4 group having exactly two bridging and two non-
621 bridging oxygens as in crystalline pyroxenes ("Q^2" groups), a wide distribution of groups with 1,
622 2, 3, and probably 0 and 4, bridging oxygens ("Q^n") (Stebbins, 1995) can be quantified by 2-
623 dimensional ^{29}Si NMR (Davis et al., 2011); one result is that the observed 1-dimensional MAS
624 NMR spectra for such glasses are typically at least 10 to 20 times broader (ca. 20 ppm) than

625 those of the corresponding crystals. Variations in bond distances and angles are also expected to
626 be large. Less is known about distributions of coordination environments for the lower-valent
627 network modifier cations, but ^{25}Mg NMR and X-ray methods have suggested that Mg^{2+} in
628 pyroxene-composition glasses probably has a mix of coordination numbers with a mean less than
629 the value of six seen in crystalline pyroxenes and olivines (George and Stebbins, 1998; Kroeker
630 and Stebbins, 2000; Trcera et al., 2009). Co^{2+} and especially Ni^{2+} have been extensively studied
631 by optical and X-ray spectroscopy and other methods in glasses including $NiCaSi_2O_6$ (Galoisy
632 and Calas, 1993; Hunault et al., 2014; Johnson et al., 1999). The short-range environments for
633 both can vary depending on glass composition, but again there are likely to be mixtures of
634 coordination numbers with means less than six: for example, the strong blue color commonly
635 caused by even <1% Co^{2+} added to silicate glasses is due to an unusually strong absorption
636 spectrum for the cation in tetrahedral coordination. M-Si distances derived from X-ray
637 spectroscopy are generally consistent with corner-shared connections. The +2 valence is
638 generally assumed to be predominant for Ni and Co in silicate glasses melted in air as done here,
639 and is consistent with optical and X-ray spectroscopic studies (Galoisy and Calas, 1993; Hunault
640 et al., 2014). However, minor concentrations of other valences, with different unpaired electron
641 spin populations, could further complicate the analysis of NMR spectra.

642 The data presented here on paramagnetic shifts in the transition metal silicate crystals of
643 known structure is (so far) too limited to uniquely address the observed large differences
644 between spectra for $MCaSi_2O_6$ glasses vs. crystals. We can say that Si environments very similar
645 to those in the clinopyroxene crystals (exclusively corner-shared octahedra, with large positive
646 shifts) are probably uncommon in the glasses. We have hypothesized that edge-sharing between
647 M^{2+} octahedra and SiO_4 tetrahedra could lead to large negative shifts, resulting in the much

smaller total shifts for the pure-phase olivines relative to the clinopyroxenes. However, it is difficult to see why a glass with a much lower ratio of M^{2+} to Si, and presumably lower bulk density, than the corresponding olivine, would have a preponderance of closely-packed edge-shared geometries.

Our data for crystalline $CoCa_2Si_2O_7$ (akermanite structure), in which all Co^{2+} is four-coordinated provides another clue: the observed paramagnetic shift is much lower than in diopside-structured $CoCaSi_2O_6$, presumably because of as-yet poorly understood differences in electronic structure and bonding. Given that low-coordinated Co^{2+} (and Ni^{2+}) are likely to be abundant in such glasses (Galoisy and Calas, 1993; Hunault et al., 2014), their much lower paramagnetic shifts may be at least in part related to this structural variable.

Paramagnetic shifts in pure phases vs. dilute solid solutions

Our previous studies of $LaPO_4$ (monazite) and YPO_4 (xenotime) doped with a few percent of rare earth ions containing unpaired electron spins (REE, e.g. Nd^{3+}, Eu^{3+}, Ce^{3+}) described paramagnetically shifted resonances corresponding to single first neighbor dopant cations in each of several distinct REE-O-P linkages (Palke and Stebbins, 2011a; Palke et al., 2013). Single-neighbor shifts of up to about 250 ppm were reported. These can be summed over each of the REE-O-P bond paths to predict what would be expected in the pure magnetic REE phase. For example, the sum over the 7 first neighbor shifts (measured at 47 ˚C, relative to the unshifted resonances at 0 ppm) in $La_{0.9}Ce_{0.1}PO_4$ is –59 ppm, and for $La_{0.9}Nd_{0.1}PO_4$ is –128 ppm (Table 1, (Palke and Stebbins, 2011a)). These totals are roughly similar to measured values of –87 for the former and –148 for the latter (correcting a typographic error in the original table). In continued studies of REE phosphates, sums of shifts observed in dilute $La_{(1-x)}Ce_xPO_4$ solid

671 solutions predicted spectra for phases with x as high as 0.33, when additional peak broadening
672 was included (Palke et al., 2013). In these examples, additivity of shifts across a wide
673 concentration range is thus a reasonable approximation and, apparently, paramagnetic
674 broadening is small enough to allow first-neighbor shifts to be readily observed in the dilute
675 solid solutions. In more detail, differences in the summed individual shifts and the total for the
676 pure phases are probably to be expected from variations in local structure with composition.
677 For our new results on pure-phase Fe, Co, Ni silicates, it is apparent that at least some
678 first-neighbor paramagnetic shifts for corner-shared M-O-Si linkages are probably on the order
679 of at least 1000 ppm, for example to account for the observed total shifts of 3000 ppm and 4400
680 ppm in $NiCaSi_2O_6$ and $CoCaSi_2O_6$ respectively. For the silicate olivines, we have hypothesized
681 that these are partially balanced by large negative shifts (also on the order of –1000 ppm) for
682 edge-shared linkages to reach the much lower total observed shifts for Ni_2SiO_4 and Co_2SiO_4 (–
683 820 and +740 ppm respectively). Without theoretical calculations, these numbers remain as only
684 initial estimates. However, the data, as well as extensive theoretical work on analogous $LiMPO_4$
685 olivines (Middlemiss et al., 2013; Pigliapochi et al., 2017), do suggest that these effects should
686 be quite large.
687 In contrast, in our recent detailed study of resolvable paramagnetically shifted ^{29}Si NMR
688 resonances in Mg_2SiO_4 with up to 5% Fe, Co, or Ni substitution (McCarty et al., 2015), we
689 detected (with conventional "one pulse" NMR methods) only much smaller shifts, up to about 50
690 to 60 ppm from the central diamagnetic peak. There, we hypothesized that some of these could
691 be attributed to first cation neighbor interactions, smaller than for transition metal phosphate
692 olivines perhaps because of more ionic bonding in the silicates. The number and relative
693 intensities of such shifted resonances also indicated that at least some were due to magnetic

694 cations in more distant shells. With the spin-echo method, somewhat faster sample spinning, and
695 variable transmitter offsets used in our new study, we did locate an additional relatively broad
696 resonance at about +135 ppm in $Mg_{1.9}Ni_{0.1}SiO_4$, but this shift (200 ppm from the diamagnetic
697 peak) is still much less than those suggested for single M-O-Si linkages in the pure phase Fe, Co,
698 and Ni olivines. Another possible discrepancy of this type may be paramagnetic shifts for ^{31}P in
699 a few transition metal lithium phosphate solid solutions, which were reported to be much smaller
700 than in the pure end member phases, for unknown reasons (Wilcke et al., 2007).

701 For the silicate olivines, this apparent discrepancy between paramagnetic shifts in the
702 dilute solid solutions and the pure paramagnetic phases could be attributed to several causes or
703 their combination. First, there could be differences in local bonding/electronic structures around
704 the transition metal cations, which, given the great sensitivity of paramagnetic shifts to structure,
705 could lead to large differences in the transfer of unpaired electron spin density to the NMR
706 nuclides in similar sites in dilute vs. pure-phase systems. Given our own results for the REE
707 phosphates as well as other examples from the battery material literature, we consider this to be
708 an unlikely explanation for overall large differences. However, it could be responsible for some
709 differences in shift magnitudes and the number and areas of shifted resonances, if occupancies of
710 sites with varying electronic structures change: for example, in the dilute olivine solutions, Ni^{2+}
711 and to some degree Co^{2+} are ordered into M1 sites in preference to M2, but occupy both M1 and
712 M2 sites in Ni_2SiO_4 and Co_2SiO_4 (Ghose and Wan, 1974; McCarty et al., 2015; Rajamani et al.,
713 1975). Secondly, it is conceivable that in the pure-phase paramagnetic olivines, there is some
714 kind of short-range magnetic ordering that greatly enhances NMR shifts relative to those in the
715 dilute systems. The transition metal silicate olivines do undergo transitions to long-range
716 magnetic ordering at low temperatures (typically <70 K (Ballet et al., 1989; Newnham et al.,

1965)), but we are aware of no evidence for continued short-range effects near room temperature. In a variable temperature ^{31}P NMR study of $LiMPO_4$ phases, large paramagnetic shifts (1000's of ppm) persisted up to at least 300 ˚C, suggesting that magnetic ordering did not be playing an important role in these materials (Wilcke et al., 2007). More generally, as concentrations of cations with unpaired electron spins increase from dilute solid solutions to pure-phase endmember, the probability of short-range magnetic interactions among them increases dramatically, conceivably leading to important effects on couplings to NMR-observed nuclei. However, any specific prediction of such effects remains a challenging theoretical problem at this point. Further studies of magnetic properties, EPR, etc., could of course contribute to resolving this hypothesis for the silicates. Thirdly, it is possible that the especially large shifts that we have observed for the Co and Ni clinopyroxenes, which are the best evidence for very large first-neighbor effects of >1000 ppm for each first neighbor M cation, are in some way anomalous, with per-cation shifts in the olivines of smaller magnitude, closer to the average values estimated above of +350 to –90 ppm/cation. Here, further studies of other end member phases (e.g. $FeCaSi_2O_6$) and of intermediate solid solutions could prove informative.

Based on this limited new data set, it now seems possible that all (instead of some) of the previously reported paramagnetic shifts in the dilute Fe, Co, Ni solid solutions in Mg_2SiO_4 (McCarty et al., 2015) are the result of cations beyond the first Si-O-M shell, with unpaired electron spin density transferred through at least four bonds (e.g. Si-O-Mg-O-Ni) and/or through space via the "pseudo-contact" mechanism. Our new data for $Mg_{1.9}Ni_{0.1}SiO_4$ (5% Ni forsterite) confirms that, apart from the newly observed +135 ppm peak, hypothesized first-neighbor paramagnetic resonances with shifts of many 100's or 1000's of ppm are not readily observable. Our measurement of the total observable peak area for this sample, of about 10 to 20% below the

740 value expected from the standard, suggests also that there are important components of the
741 spectrum that are not detected by the methods used. However, a simple probability calculation
742 (McCarty et al., 2015; McCarty and Stebbins, 2016b) for this composition, assuming all Ni^{2+}
743 cations are on the M1 site, predicts that 66% of the Si have no Ni^{2+} in the first shell. If all signals
744 from Si with one or more first shell Ni^{2+} are missed in the NMR spectra, an overall signal loss of
745 34% is thus expected. The observed loss is considerably less than this, although uncertainties are
746 fairly large. It could be that the newly-detected resonance at +135 ppm is indeed due to one
747 corner-shared first neighbor coupling that is relatively small compared to our estimates from the
748 end member transition metal silicates, or that some combination of paramagnetic shifts from
749 first-neighbor cations results in intensity within the observed manifold of peaks. Again, the
750 possibility that paramagnetic shifts deduced from the pure-phase samples do not accurately
751 predict the observations in dilute solid solutions could be clarified by further study of
752 intermediate compositions.

753 This apparent loss of some observable signal for Si with first-neighbor paramagnetic
754 cations in the Ni-doped forsterite seems surprising, given the readily observable spectra for the
755 pure-phase materials, with peak areas approximately as expected from standardization, and spin-
756 spin relaxation times T_2 long enough to avoid major signal losses during the spin echo delay
757 time. The relatively low intensity of such resonances in the dilute systems, and possible
758 broadening due to disorder, of course contributes to this problem, but our observations suggests
759 that additionally, signal decay and/or peak broadening caused by rapid relaxation may be
760 unusually severe in the magnetically more dilute silicate minerals. For the 5% Ni forsterite, the
761 systematically shorter T_2 values for the observed resonances that result from stronger Ni-Si
762 interactions (larger shifts) imply the possibility of even shorter values for hypothesized first-

neighbor interactions with even larger paramagnetic shifts. This could lead to signal loss during the NMR acquisition, and/or more severe peak broadening, making direct detection of such signals difficult, especially when their intensities are small in dilute solutions.

We do not yet have a definitive explanation for the unusually short T_2 values for the highly-shifted resonances in the more dilute Ni silicates, but note that for the pure phases studied here, T_2 is shortest in one of the minerals that has the *lowest* transition metal contents ($NiCaSi_2O_6$). In our recent report on ^{29}Si NMR of Cu(II) silicates (Stebbins, 2017), we noted that the only one of the minerals studied for which T_2 was short enough to lead to major signal loss was that with the lowest Cu content, cuprorivaite ($CaCuSi_4O_{10}$). We speculated that this could be the result of reduced magnetic Cu-Cu interactions, as this phase has isolated Cu^{2+} ions instead of chains of Cu^{2+} in minerals such as dioptase ($Cu_6Si_6O_{18}$-$6H_2O$). This effect might in turn lead to longer electron spin-lattice relaxation times, possibly enhancing the efficiency of coupling of unpaired electron spins to nuclear spins and actually shortening the nuclear spin relaxation time. We have no direct evidence to support this hypothesis for other transition metal silicates, but it could be an important part of the difference in behavior between dilute and concentrated systems.

The MAS data for the San Carlos olivine ($Mg_{1.8}Fe_{0.2}SiO_4$) provide another window onto this complex problem. Relative to the $Mg_{1.9}Ni_{0.1}SiO_4$ olivine, this mineral has twice the concentration of paramagnetic cations and these are probably distributed over both M1 and M2 sites instead of occupying primarily M1. Importantly, Fe^{2+} has 4 unpaired electron spins, Ni^{2+} only 2. Both concentration and spin numbers probably contribute to the much greater broadening of the MAS-resolved resonances (ca. 2 ppm FWHM for the Ni solid solution, 75 ppm for the Fe sample); conversely, however, the very broad, unresolved component for strongly-interacting

sites is detectable in the latter but not the former. A simple probability calculation for the $Mg_{1.8}Fe_{0.2}SiO_4$ composition predicts 39% of the Si with no Fe^{2+} in first-neighbor positions, which corresponds roughly with the estimate of 35±5% of the total area in the narrower component of the composite static (or MAS) spectra. However, even the very broad observed component seems to span a smaller range of shifts than suggested by our crude estimates for individual bond path contributions described above, which are least well constrained for Fe^{2+} relative to Ni^{2+} or Co^{2+}**,** given data for only a single pure-phase Fe silicate at this time. A relatively rapid spin-spin relaxation (short T_2) is also seen for the broad component of the San Carlos olivine spectra, although in this case this effect apparently does not lead to a large loss in total observable signal.

Implications

Since the first widespread application of ^{29}Si NMR to silicate minerals and glasses in the early- to mid-1980's, the method has become one of our most important experimental tools for quantifying questions of short- to medium-range structure in materials with significant variations from perfect ordering (Kirkpatrick 1988; MacKenzie and Smith, 2002; Stebbins and Xue, 2014). Because order/disorder is a key issue in the crystalline solid solutions that are nearly ubiquitous in natural and in technological systems, and is even more fundamental to the nature and properties of glasses and liquids, NMR has had a major impact in our understanding of the molecular-scale details that control many different processes. However, almost all of such studies have been limited to materials with relatively low concentrations of ions with unpaired electron spins, as early work suggested that minerals with more than a few percent of such magnetic transition metal or rare earth cations would yield uninterpretable or even unobservable

spectra (Grimmer et al., 1983). Large ranges of composition of geologically and technologically important materials have thus been excluded from study by NMR on this important nuclide, as well as others of particular mineralogical interest such as ^{27}Al and ^{17}O. The most important implication of our new study, along with our initial work on Cu(II) silicates (Stebbins, 2017), is thus to demonstrate that ^{29}Si NMR experiments on silicate minerals and glasses with high concentrations of paramagnetic transition metal cations can indeed provide informative spectra, despite considerable challenges in data collection and interpretation. Although this type of application of NMR is in its infancy, the potential expansion in the scope of the method offers a wide range of future exploration and potential discovery of new insights into structure in crystalline and amorphous solids.

In more technical detail, the results presented here have important implications for the methods needed to obtain useful data, for the types of systems where future work may be most feasible, and for what needs to be developed to make progress in a challenging new field. For the olivines, clinopyroxenes, and glasses studied here, we have found that spin-spin relaxation times (T_2) are generally long enough to allow quantitative acquisition of spectra, although peak broadening can be severe and spectra are shifted far outside of the range generally observed for diamagnetic silicates. Large effects of variation in short range structure and composition on observable paramagnetic shifts, line widths, and relaxation processes suggest a sensitive new approach for understanding more about bonding, electronic, and magnetic structure. Although unique interpretations of these data are also difficult at this early stage of our knowledge, future systematic experimental studies of individual transition metal substitutions over a wider range of known structures and solid solutions are likely to be revealing of systematic trends in effects of

variables such as number of unpaired electron spins, cation coordination numbers, edge- vs. corner-shared bonding, and structural and magnetic order/disorder.

Spectra for transition metal rich silicate glasses are extremely broad and time-consuming to observe, but careful analysis of integrated peak intensities indicates that they can be accurately measured. At least for the $NiCaSi_2O_6$ and $CoCaSi_2O_6$ compositions, the peak widths and positions are very different from those of the corresponding crystals, requiring major differences in structural order and average short range structure, probably due in part to differences in transition metal cation coordination numbers. Again, future, more systematic studies are likely to provide new insights into the many remaining unknowns of silicate glass and melt structure.

Our new results for pure-phase Fe, Co and Ni silicate minerals suggest that paramagnetic shifts in ^{29}Si NMR spectra caused by single transition metal cation neighbors may be much larger (100's to 1000's of ppm) than any of the resolved, shifted resonances detected in our recent work on forsterite (Mg_2SiO_4) containing up to a few percent of these substituents (McCarty et al., 2015). This implies that signals for such first-neighbor pairs may be especially difficult to detect in dilute solid solution because of rapid relaxation and/or severe broadening of such low-intensity features of the spectra. Independent evidence for this possibility comes from new observations of especially rapid spin-spin relaxation (and thus signal decay during the NMR experiment) for resonances with large shifts and/or broadening in a forsterite with a 5% Ni_2SiO_4 component and in natural San Carlos olivine (10% Fe_2SiO_4 component). This conclusion implies that some re-interpretation of our previous data on the dilute solid solutions may provide additional information on cation ordering in olivine. Furthermore, the large numbers of well-resolved, observable resonances in the spectra of dilute silicate solid solutions (McCarty et al., 2015) may present unique opportunities to better understand extended cation ordering, if

paramagnetic shifts are actually dominated by second neighbor (or even longer-range) interactions.

Beyond the further development of empirical correlations between short-range structure and NMR observables, future NMR studies of ^{29}Si (and other nuclides) in paramagnetic-rich silicates are likely to be considerably enhanced by more advanced methodologies, including more complex pulse sequences that more effectively excite very broad resonances (Pell and Pintacuda, 2015) and MAS probes that can spin samples to much higher frequencies. Probably most importantly, the coupling of experimental work with advanced computational approaches, as has been so-well demonstrated for transition-metal rich Li phosphate battery materials (Pecher et al., 2017; Pigliapochi et al., 2017) has the potential to provide unique and detailed connections between spectra and short-range structure in a host of complex and incompletely known materials.

Acknowledgements

This research was supported by the National Science Foundation, EAR-1521055. We thank Dale Burns (Stanford University) for the electron microprobe analyses. The paper was improved by helpful comments from two anonymous reviewers.

References

Abrahams, I., and Easson, K.S. (1993) Structure of lithium nickel phosphate. Acta Crystallographica C, C49, 925-926.

Ballet, O., Fuess, H., Wacker, K., Untersteller, E., Treutmann, W., Hellner, E., and Hosoya, S. (1989) Magnetisation measurements of the synthetic olivine single crystals A_2SiO_4 with A=Mn, Fe or Co. Journal of Physics: Condensed Matter, 1, 4955-4970.

Begaudeau, K., Morizet, Y., Florian, P., Paris, M., and Mercier, J.-C. (2012) Solid-state NMR analysis of Fe-bearing minerals: implications and applications for Earth sciences. European Journal of Mineralogy, 24, 535-550.

Carlier, D., Ménétrier, M., Grey, C.P., Delmas, C., and Ceder, G. (2003) Understanding the NMR shift in paramagnetic transition metal oxides using density functional theory. Physical Review, 67, 174103-1-14.

Clément, R.J., Pell, A.J., Middlemiss, D.S., Strobridge, F.C., Miller, J.K., Whittingham, M.S., Emsley, L., Grey, C.P., and Pintacuda, G. (2012) Spin-transfer pathways in paramagnetic lithium transition-metal phosphates from combined broadband isotropic solid-state MAS NMR spectroscopy and DFT calculations. Journal of the American Chemical Society, 134, 17178-17185.

Dajda, N., Dixon, J.M., and Smith, M.E. (2003) Atomic site preferences and structural evolution in vanadium-doped $ZrSiO_4$ from multinuclear solid-state NMR. Physical Review B, 67, 024201-1-024201-9.

894 Davis, M.C., Sanders, K.J., Grandinetti, P.J., Gaudio, S.J., and Sen, S. (2011) Structural
895 investigations of magnesium silicate glasses by ^{29}Si 2D magic-angle flipping NMR.
896 Journal of Non-Crystalline Solids, 357, 2787-2795.
897 Durand, G., Vilminot, S., Rabu, P., Derory, A., and Lambour, J.P. (1996) Synthesis, structure,
898 and magnetic properties of $CaMSi_2O_6$ (M=Co,Ni) compounds and their solid solutions.
899 Journal of Solid State Chemistry, 124, 374-380.
900 Engelhardt, G., and Michel, D. (1987) High-Resolution Solid-State NMR of Silicates and
901 Zeolites. 485 p. Wiley, New York.
902 Galoisy, L., and Calas, G. (1993) Structural environment of nickel in silicate glass/melt systems:
903 Part I. Spectroscopic determinations of coordination states. Geochimica et Cosmochimica
904 Acta, 57, 3613-3626.
905 George, A.M., and Stebbins, J.F. (1998) Structure and dynamics of magnesium in silicate melts:
906 a high temperature ^{25}Mg NMR study. American Mineralogist, 83, 1022-1029.
907 George, N.C., Pell, A.J., Dantelle, G., Page, K., Llobet, A., Balasubramanian, M., Pintacuda, G.,
908 Chmelka, B.F., and Seshadri, R. (2013) Local environments of dilute activator ions in the
909 solid-state lighting phosphor $Y_{3-x}Ce_xAl_5O_{12}$. Chemistry of Materials, 25, 3979-3995.
910 Ghose, S., and Wan, C. (1974) Strong site preference of Co^{2+} in olivine, $Co_{1.10}Mg_{0.90}SiO_4$.
911 Contributions to Mineralogy and Petrology, 47, 131-140.
912 Ghose, S., Wan, C.e., and Okamura, F.P. (1987) Crystal structures of $CaNiSi_2O_6$ and $CaCoSi_2O_6$
913 and some crystal-chemical relations in C2/x clinopyroxenes. American Mineralogist, 72,
914 375-381.

915 Grey, C.P., Dobson, C.M., Cheetham, A.K., and Jakeman, R.J.B. (1989) Studies of rare-earth
916 stannates by ^{119}Sn MAS NMR. The use of parmagnetic shift probes in the solid state.
917 Journal of the American Chemical Society, 111, 505-511.
918 Grey, C.P., and Dupré, N. (2004) NMR studies of cathode materials for lithium-ion rechargeable
919 batteries. Chemical Reviews, 104, 4493-4512.
920 Grey, C.P., Smith, M.E., Cheetham, A.K., Dobson, R., and Dupree, R. (1990) Y-89 MAS NMR
921 study of rare-earth pyrochlores-paramagnetic shifts in the solid state. Journal of the
922 American Chemical Society, 112, 4670-4680.
923 Grimmer, A.-R., von Lampe, F., Mägi, M., and Lippmaa, E. (1983) Hochauflösende ^{29}Si-NMR
924 an festen Silicaten; Einfluss von Fe^{2+} in Olivinen. Zeitschrift für Chemie, 23, 343-344.
925 Hartman, J.S., Narayanan, A., Rigby, S.S., Sliwinski, D.R., Halden, N.M., and Bain, A.D. (2007)
926 Heterogeneities in sol-gel-derived paramagnetics-doped forsterites and willemites-
927 Electron microprobe analysis and stretched-exponential ^{29}Si NMR spin-lattice relaxation
928 studies. Canadian Journal of Chemistry, 85, 56-65.
929 Hunault, M., Calas, G., Galoisy, L., LeLong, G., and Newville, M. (2014) Local ordering around
930 tetrahedral Co^{2+} in silicate glasses. Journal of the American Ceramic Society, 97, 60-62.
931 Johnson, J.A., Johnson, C.E., Holland, D., Mekki, A., Appleyard, P., and Thomas, M.F. (1999)
932 Transition metal ions in ternary sodium silicate glasses: a Mössbauer and neutron study.
933 Journal of Non-Crystalline Solids, 246, 104-114.
934 Kim, J., Ilott, A.J., Middlemiss, D.S., Chenova, N.A., Pinney, N., Morgan, D., and Grey, C.P.
935 (2015) ^{2}H and ^{27}Al solid-state NMR study of the local environments in Al-doped 2-line
936 ferrihydrite, goethite, and lepidocrocite. Chemistry of Materials, 27, 3966-3978.

937 Kim, J., Li, W., Phillips, B.L., and Grey, C.P. (2011) Phosphate adsorption on the iron
938 oxyhydroxides goethite (α-FeOOH), akaganite (β-FeOOH), and lepidocrocite (γ-
939 FeOOH): a ^{31}P NMR study. Energy and Environmental Science, 4, 4298-4305.
940 Kim, J., Middlemass, D.S., Chernova, N.A., Zhu, B.X.Y., Masquelier, C., and Grey, C.P. (2010)
941 Linking local environments and hyperfine shifts: A combined experimental and
942 theoretical ^{31}P and ^{7}Li solid-state NMR study of paramagnetic Fe(III) phosphates. Journal
943 of the American Chemical Society, 132, 16825-16840.
944 Kirkpatrick, R.J. (1988) MAS NMR spectroscopy of minerals and glasses. In F.C. Hawthorne,
945 Ed. Spectroscopic Methods in Mineralogy and Geology, p. 341-403. Mineralogical
946 Society of America, Washington D.C.
947 Kroeker, S., and Stebbins, J.F. (2000) Magnesium coordination environments in glasses and
948 minerals: New insight from high field magnesium-25 MAS NMR. American
949 Mineralogist, 85, 1459-1464.
950 Kusaka, K., Hagiya, K., Ohmasa, M., Okano, Y., Mukai, M., Iishi, K., and Haga, N. (2001)
951 Determination of structures of $Ca_2CoSi_2O_7$, $Ca_2MgSi_2O_7$, and $Ca_2(Mg_{0.55}Fe_{0.45})Si_2O_7$ in
952 incommensurate and normal phases and observation of diffuse streaks at high
953 temperature. Physics and Chemistry of Minerals, 28, 150-166.
954 MacKenzie, K.J.D., and Smith, M.E. (2002) Multinuclear Solid-State NMR of Inorganic
955 Materials. 727 p. Pergamon, New York.
956 McCarty, R.J., Palke, A.C., Stebbins, J.F., and Hartman, J.S. (2015) Transition metal cation site
957 preferences in forsterite (Mg_2SiO_4) determined from paramagnetically shifted NMR
958 resonances. American Mineralogist, 100, 1265-1276.

McCarty, R.J., and Stebbins, J.F. (2016a) Investigating lanthanide dopant distributions in yttrium aluminum garnet (YAG) using solid state paramagnetic NMR. Solid State Nuclear Magnetic Resonance, 79, 11-22.

-. (2016b) Transition metal dopant cation distributions in MgO and CaO: new inferences from paramagnetic shifts in ^{17}O, ^{25}Mg and ^{43}Ca NMR spectra. Journal of Physical Chemistry C, 120, 11111-11120.

Middlemiss, D.S., Ilott, A.J., Clément, R.J., Strobridge, F.C., and Grey, C.P. (2013) Density functional theory-based bond pathway decompositions of hyperfine shifts: equipping solid-state NMR to characterize atomic environments in paramagnetic materials. Chemistry of Materials, 25, 1723-1734.

Navrotsky, A., and Coons, W.E. (1976) Thermochemistry of some pyroxenes and related compounds. Geochimica et Cosmochimica Acta, 40, 1281-1288.

Newnham, R., Santoro, R., and Nomura, S. (1965) Antiferromagnetism in nickel orthosilicate. Acta Crystallographica, 19, 147-148.

O'Neill, H.S.C. (1987) Free energies of formation of NiO, CoO, Ni_2SiO_4, and Co_2SiO_4. American Mineralogist, 72, 280-291.

Palke, A.C., and Stebbins, J.F. (2011a) Paramagnetic interactions in the ^{31}P NMR spectroscopy of rare earth element orthophosphate ($REPO_4$, monazite/xenotime) solid solutions. American Mineralogist, 96, 1343-1353.

-. (2011b) Variable temperature ^{27}Al and ^{29}Si NMR studies of synthetic forsterite and Fe-bearing Dora Maira pyrope garnet: temperature dependence and mechanisms of contact-shifted peaks. American Mineralogist, 96, 1090-1099.

Palke, A.C., Stebbins, J.F., and Boatner, L.A. (2013) ^{31}P MAS-NMR study of flux-grown rare-earth element orthophosphate (monazite/xenotime) solid solutions: evidence for random cation distribution from paramagnetically shifted NMR resonances. Inorganic Chemistry, 52, 12605-12615.

Palke, A.C., Stebbins, J.F., Geiger, C.A., and Tippelt, G. (2015) Cation order-disorder in Fe-bearing pyrope and grossular garnets: An ^{27}Al and ^{29}Si MAS NMR and ^{57}Fe Mössbauer spectroscopy study. American Mineralogist, 100, 536-547.

Pecher, O., Carretero-Gonzalez, J., Griffith, K.J., and Grey, C.P. (2017) Materials' methods: NMR in battery research. Chemistry of Materials, 29, 213-242.

Pell, A.J., and Pintacuda, G. (2015) Broadband solid-state MAS NMR of paramagnetic systems. Progress in Nuclear Magnetic Resonance, 84-85, 33-72.

Pigliapochi, R., Pell, A.J., Seymour, I.D., and Grey, C.P. (2017) DFT investigation of the effect of spin-orbit coupling on the NMR shifts in paramagnetic solids. Physical Review A, 95, 054412-1-11.

Puphal, P., Sheptyakov, D., van Well, N., Postulka, L., Heinmaa, I., Ritter, F., Assmus, W., Wolf, B., Lang, M., Jeschke, H.O., Valenti, R., Stern, R., Rüegg, C., and Krellner, C. (2016) Stabilization of the tetragonal structure in $(Ba_{1-x}Sr_x)CuSi_2O_6$. Physical Review B, 93, 174121-1-9.

Rajamani, V., Brown, G.E., Jr., and Prewitt, C.T. (1975) Cation ordering in Ni-Mg olivine. American Mineralogist, 60, 292-299.

Raudsepp, M., Hawthorne, F.C., and Turnock, A.C. (1990) Crystal chemistry of synthetic pyroxenes on the join $CaNiSi_2O_6$-$CaMgSi_2O_6$ (diopside). American Mineralogist, 75, 1274-1281.

1004 Saji, H., Yamadaya, T., and Asanuma, M. (1973) Nuclear magnetic resonances of ^{29}Si and long-
1005 range superexchange interactions via Co-O-Si-O-Co linkages in Co_2SiO_4. Physics
1006 Letters, 45A, 109-110.
1007 Sherriff, B.L., and Hartman, J.S. (1985) Solid-state high-resolution ^{29}Si NMR of feldspars: Al-Si
1008 disorder and the effects of paramagnetic centres. Canadian Mineralogist, 23, 205-212.
1009 Smyth, J.R. (1975) High temperature crystal chemistry of fayalite. American Mineralogist, 60,
1010 1092-1097.
1011 Stebbins, J.F. (1995) Dynamics and structure of silicate and oxide melts: nuclear magnetic
1012 resonance studies. In J.F. Stebbins, P.F. McMillan, and D.B. Dingwell, Eds. Structure,
1013 Dynamics, and Properties of Silicate Melts, 32, p. 191-246. Mineralogical Society of
1014 America, Washington, D.C.
1015 Stebbins, J.F. (2017) Towards the wider application of ^{29}Si NMR spectroscopy to paramagnetic
1016 transition metal silicate minerals: copper(II) silicates. American Mineralogist, 102, 2406-
1017 2414.
1018 Stebbins, J.F., and Kelsey, K.E. (2009) Anomalous resonances in ^{29}Si and ^{27}Al NMR spectra of
1019 pyrope ($[Mg,Fe]_3Al_2Si_3O_{12}$) garnets: effects of paramagnetic cations. Physical Chemistry
1020 Chemical Physics, 11, 6906-6917.
1021 Stebbins, J.F., McCarty, R.J., and Palke, A.C. (2017) Solid-state NMR and short-range order in
1022 crystalline oxides and silicates: a new tool in paramagnetic resonances. Acta
1023 Crystallographica C, 73, 128-136.
1024 Stebbins, J.F., Smyth, J.R., Panero, W.R., and Frost, D.J. (2009) Forsterite, hydrous and
1025 anhydrous wadsleyite and ringwoodite (Mg_2SiO_4): ^{29}Si NMR results for chemical shift

anisotropy, spin-lattice relaxation, and mechanism of hydration. American Mineralogist, 94, 905-915.

Stebbins, J.F., and Xue, X. (2014) NMR spectroscopy of inorganic Earth materials. In G.S. Henderson, D. Neuville, and R.T. Downs, Eds. Spectroscopic Methods in Mineralogy and Materials Sciences, 78, p. 605-653. Min. Soc. Am., Chantilly, VA.

Strobridge, F.C., Middlemiss, D.S., Pell, A.J., Leskes, M., Clément, R.J., Pourpoint, F., Lu, Z., Hanna, J.V., Pintacuda, G., Emsley, L., Samosen, A., and Grey, C.P. (2014) Characterizing local environments in high energy density Li-ion battery cathodes: a combined NMR and first principles study of $LiFe_xCo_{1-x}PO_4$. Journal of Materials Chemistry A, 2, 11948-11957.

Sugawara, T., and Akaogi, M. (2003) Calorimetric measurements of fusion enthalpies for Ni_2SiO_4 and Co_2SiO_4 olivines and applications to olivine-liquid partitioning. Geochimica et Cosmochimica Acta, 67, 2683-2693.

Takahashi, T., Kawashima, H., Sugisawa, H., and Baba, T. (1999) ^{207}Pb chemical shift thermometer at high temperature for magic angle spinning experiments. Solid State Nuclear Magnetic Resonance, 15, 119-123.

Tamada, O., Fujino, K., and Sasaki, S. (1983) Structures and electron distributions of a-Co_2SiO_4 and a-Ni_2SiO_4 (olivine structure). Acta Crystallographica B, B39, 692-697.

Trcera, N., Cabaret, D., Rossano, S., Farges, F., Flank, A.-M., and Lagarde, P. (2009) Experimental and theoretical study of the structural environment of magnesium in minerals and silicate glasses using X-ray absorption near-edge structure. Physics and Chemistry of Minerals, 36, 241-257.

1048 Tucker, M.C., Doeff, M.M., Richardson, T.J., Finones, R., Reimer, J.A., and Carirns, E.J. (2002)
1049 ^{7}Li and ^{31}P magic angle spinning nuclear magnetic resonance of $LiFePO_4$-type materials.
1050 Electrochemical and Solid-State Letters, 5, A95-A98.
1051 Wilcke, S.L., Lee, Y.-J., Cairns, E.J., and Reimer, J.A. (2007) Covalency measurements via
1052 NMR in lithium metal phosphates. Applied Magnetic Resonace, 32, 547-563.
1053 Yoon, W.S., Iannopollo, S., Grey, C.P., Carlier, D., Gorman, J., Reed, J., and Ceder, G. (2004)
1054 Local structure and cation ordering in O3 lithium nickel manganese oxides with
1055 stoichiometry $Li[Ni_xMn_{(2-x)/3}Li_{(1-2x)/3}]O_2$. Electrochemical and Solid-State Letters, 7,
1056 A167-A171.
1057 Zeng, D., Cabana, J., Bréger, J., Yoon, W.S., and Grey, C.P. (2007) Cation ordering in
1058 $Li[Ni_xMn_xCo_{(1-2x)}]O_2$ layered cathode materials: a nuclear magnetic resonance (NMR),
1059 pair distribution function, X-ray absorption, and electrochemical study. Chemistry of
1060 Materials, 19, 6277-6289.
1061
1062

Table 1. Pure-phase crystalline silicates studied here: summary of first neighbor cation bond paths and NMR results from static spectra for these and for glasses. Here, as throughout paper, "M" denotes paramagnetic +2 transition metal cation.

composition (structure type)	no. of M first neighbors to Si	no. of unpaired electrons per M	no. of M-O-Si paths, corner-shared	no. of M-O-Si paths, edge-shared	^{29}Si NMR shift, ppm (mean isotropic shift)	width, FWHM in ppm[a]
$NiCaSi_2O_6$ (diopside)	3	2	3	0	3000	580
$NiCaSi_2O_6$ (glass)					700	2000
$CoCaSi_2O_6$ (diopside)	3	3	3	0	4400	1700
$CoCaSi_2O_6$ (glass)					1200	3700
Ni_2SiO_4 (olivine)	9	2	6	6[b]	–820	1250
Co_2SiO_4 (olivine)	9	3	6	6 [b]	740	2100
Fe_2SiO_4 (olivine)	9	4	6	6 [b]	3200	2500
$CoCa_2Si_2O_7$[c] (akermanite)	2	3	2	0	1380	1400

Notes:

[a] Full width at half maximum (FWHM) is only a rough description of the width for asymmetric peak shapes such as those observed here: see figures.

[b] Note that each M cation in an edged-shared site contributes two M-O-Si bond paths to each adjacent Si.

[c] Four, instead of six-coordinated, transition metal cation as in olivine and pyroxene crystals

Table 2. Spin-spin relaxation time data and corrected ^{29}Si NMR peak areas

composition	phase or peak	T_2, μs	% signal loss in standard echo time[b]	corrected total peak area, per mg of SiO_2[c]
Ni_2SiO_4	crystal	1700[a]	6	20.3
Co_2SiO_4	crystal	1400[a]	7	20.2
Fe_2SiO_4	crystal	1100[a]	9	18.5[d]
$CoCa_2Si_2O_7$	crystal	750[a]	13	20.8
$NiCaSi_2O_6$	crystal	500[a]	18	18.9
	glass	1650[e]	6	18.2
$CoCaSi_2O_6$	crystal	1600[a]	6	18.7
	glass	1800[f]	6	18.2
$Mg_{1.8}Fe_{0.2}SiO_4$	olivine,[g] MAS	2100[a]	5	17.8
	static	1600[f]	6	18.5
	static, offset	650[h]	15	-
$Mg_{1.}Ni_{0.1}SiO_4$	MAS, center pk	5600	2	15.0 (all)[i]
	MAS, –40 ppm pk	1500	6	
	MAS, +135 ppm pk	200	56	
	static	900	11	16.9
$MgCaSi_2O_6$	crystal[j]	-	≈ 0	19.0

Notes:

[a] data are for the transmitter frequency centered near the most intense component of the line shape

[b] 2 MAS rotor periods: 100 μs for all but $Mg_{1.}Ni_{0.1}SiO_4$ where 91 μs was used to match 22 kHz spin rate

[c] uncertainties in areas about 10%

[d] area is minimum value, not corrected for roughly 5-10% excess crystalline silica (see text)

[e] data for two largest components of spectrum

[f] data for entire composite spectrum

[g] from peridotite nodule, San Carlos, NM

[h] data for component centered 200 kHz (2500 ppm) above peak maximum

[i] corrected with mean value for all observed peaks, 6% total signal loss

[j] high-purity diopside standard, Wakefield, Quebec

Figure captions

Figure 1. ^{29}Si spin echo spectra for Ni_2SiO_4, comparing results for static (non-spinning) sample vs. MAS at 20 kHz spinning rate. The static spectrum is the sum of two spectra collected with transmitter frequency shifted by 100 kHz (1260 ppm); the MAS data were collected at a single transmitter setting near to the highest peak.

Figure 2. ^{29}Si spin echo spectra for $NiCaSi_2O_6$ and $CoCaSi_2O_6$, collected with 20 kHz MAS and a single transmitter setting for each, centered near the peak maximum. Especially for the latter, the full peak width is not accurately recorded because of the limited excitation bandwidth.

Figure 3. Central regions of ^{29}Si spin echo MAS spectra for Ni_2SiO_4, comparing results for sample spinning at different rates as labeled. The most likely location of the central peak, marking the isotropic chemical shift (δ_{iso}), is marked by the dashed line: its position shifts towards the diamagnetic value (ca. –61 ppm) with increasing temperature, the latter due to rotational air friction. All other peaks are spinning sidebands, separated by the spinning frequency. An example of a full spectrum in shown in Fig. 1.

Figure 4. ^{29}Si spin echo static (non-spinning) spectra for Fe_2SiO_4 (fayalite), Co_2SiO_4, and Ni_2SiO_4, showing summed spectra only for clarity. Centers of gravity, marking the isotropic shifts, are marked and labeled. Spectra collected at four transmitter frequencies successively offset by 100 kHz and summed are illustrated for Co_2SiO_4. The known range of isotropic and

anisotropic chemical shifts for SiO_4 groups in diamagnetic silicates is shown by the box with dashed lines.

Figure 5. ^{29}Si spin echo spectra for crystalline and glassy $NiCaSi_2O_6$. For the glass, both MAS and static spectra are shown, revealing a minor component with much lower paramagnetic shift and broadening than the bulk of the sample. Centers of gravity, marking the mean isotropic shifts, are marked and labeled. The arrow labeled "Ol" shows the center of the peak for Ni_2SiO_4 olivine.

Figure 6. ^{29}Si spin echo static spectra for crystalline and glassy $CoCaSi_2O_6$, and crystalline $CoCa_2Si_2O_7$. Centers of gravity, marking the mean isotropic shifts, are marked and labeled. The arrow labeled "Ol" shows the center of the peak for Co_2SiO_4 olivine.

Figure 7. ^{29}Si spin echo spectra for San Carlos olivine (ca. $Mg_{1.8}Fe_{0.2}SiO_4$) collected with MAS at 20 and 22 kHz. "A" marks the most prominent, narrowed peak whose position is shifted only slightly from that of forsterite. (The position and width of the latter are marked by the vertical line labeled "Fo100"). "B" and "B?" mark possible positions of a second, partially resolved peak that has a significant paramagnetic shift: these are separated by close to the 22 kHz spinning rate and one is probably a sideband of the other. "*" marks obvious spinning sidebands. The central regions are shown in the larger spectra; the full, composite spectrum (22 kHz) is shown in the inset on a different scale.

Figure 8. ^{29}Si spin echo spectra for olivine solid solutions. Upper three are for San Carlos olivine (ca. $Mg_{1.8}Fe_{0.2}SiO_4$), comparing the static spectrum with the MAS spectrum (as in Fig. 7 but with an enlarged vertical scale factor). The upper curve (black) shows the data collected under standard conditions with spin echo delay τ of 100 μs, the lower overlaid curve (blue) shows data for τ of 700 μs. The lower pair shows the static spectrum for 5%Ni forsterite ($Mg_{1.9}Ni_{0.1}SiO_4$) with two different vertical scale factors to illustrate the absence of a detectable broad component.

Figure 9. ^{29}Si spin echo spectra for 5%Ni forsterite ($Mg_{1.9}Ni_{0.1}SiO_4$) collected with MAS at 22 kHz. Inset (on a different frequency scale and offset to the right) shows the newly-observed peak at about +135 ppm, with vertical scale about 20x that of central region shown below. * marks a spinning sideband. In each plot, three spectra are overlaid, collected with echo delay τ of 91μs (highest intensities) to 273 to 909 μs (lowest).

Figure 10. Plot of the natural logarithm of the observed NMR peak area ratioed to the area at the shortest echo delay tested (60 or 100 μs), vs. echo delay, for Ni-containing crystals, illustrating variation in T_2 (the inverse of the slope) as listed in Table 2.

Figure 11. Plot of isotropic paramagnetic shifts observed near to room temperature for transition metal silicates and lithium phosphates, vs. number of unpaired electron spins for each M^{2+} cation. Solid circles are published data for ^{31}P shifts in $LiMPO_4$ (M= Fe^{2+}, Co^{2+}, Ni^{2+}) olivines (Wilcke et al., 2007). Squares mark ^{29}Si shifts for M_2SiO_4 olivines; triangles show data for $MCaSi_2O_6$ clinopyroxenes.

Figure 12. Local structures around the SiO_4 tetrahedra in M_2SiO_4 olivine and $MCaSi_2O_6$ clinopyroxene. Apart from the central Si and its 4 first neighbor O (red), only cation sites that may be occupied by Fe^{2+}, Co^{2+} or Ni^{2+} are shown: 4 M1 (green) and 5 M2 (brown) sites for olivine, 3 M1 (green) sites for clinopyroxene. M-O-Si bond paths for corner-shared octahedra are shown in gray, those for edge-shared octahedra are highlighted by dashed lines (color online).

Figure 1

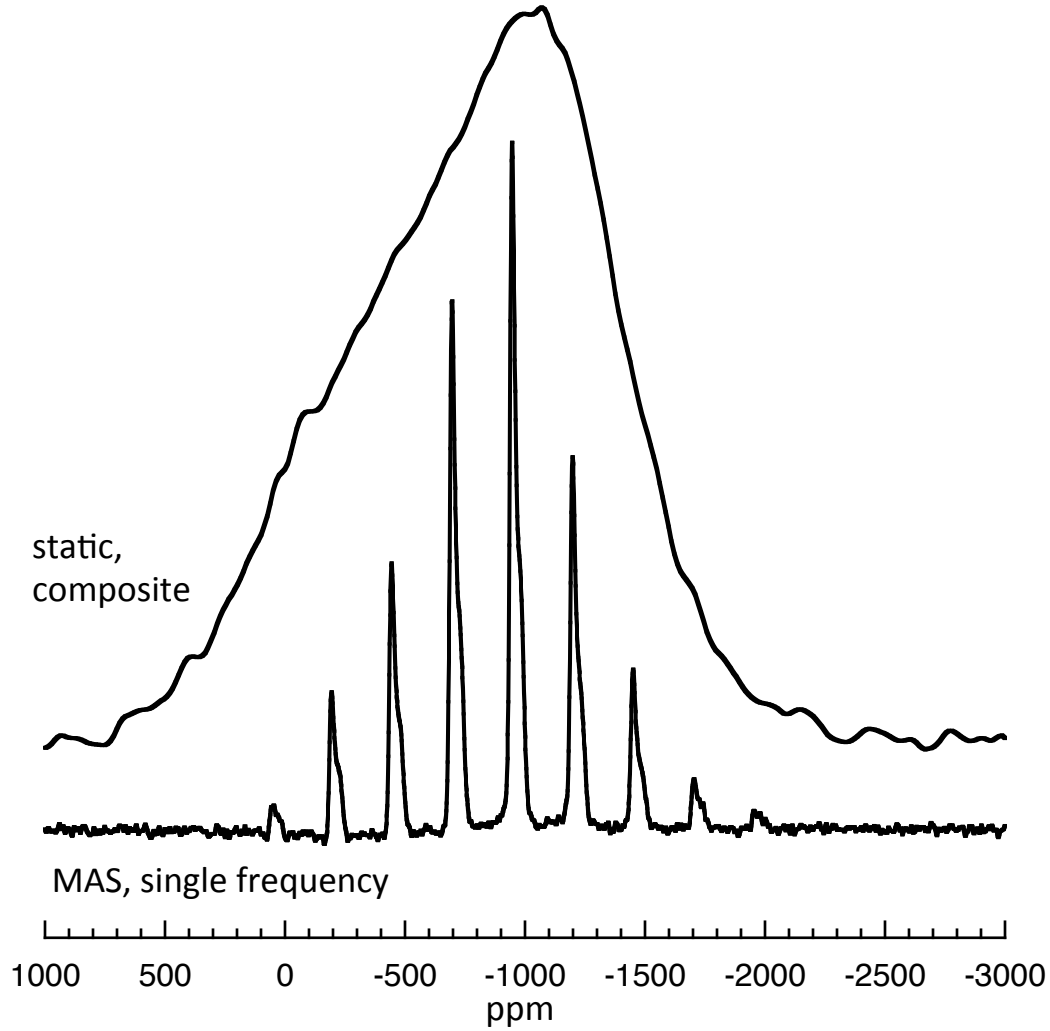
static,
composite
MAS, single frequency
1000
500
0
-500
-1000
-1500
-2000
-2500
-3000
ppm

Figure 2

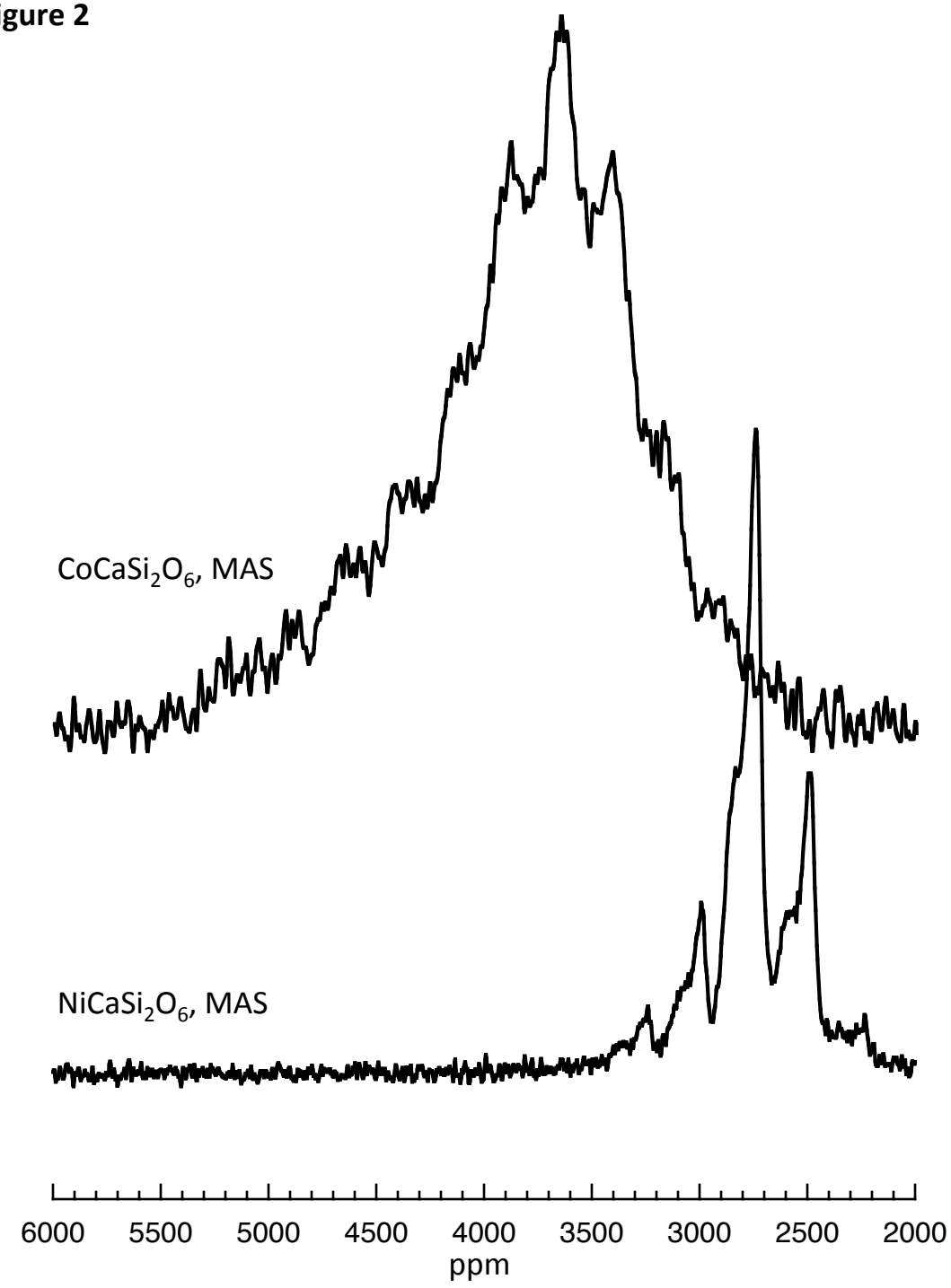
CoCaSi2O6, MAS
NiCaSi2O6, MAS
6000
5500
5000
4500
4000
3500
3000
2500
2000
ppm

Figure 3

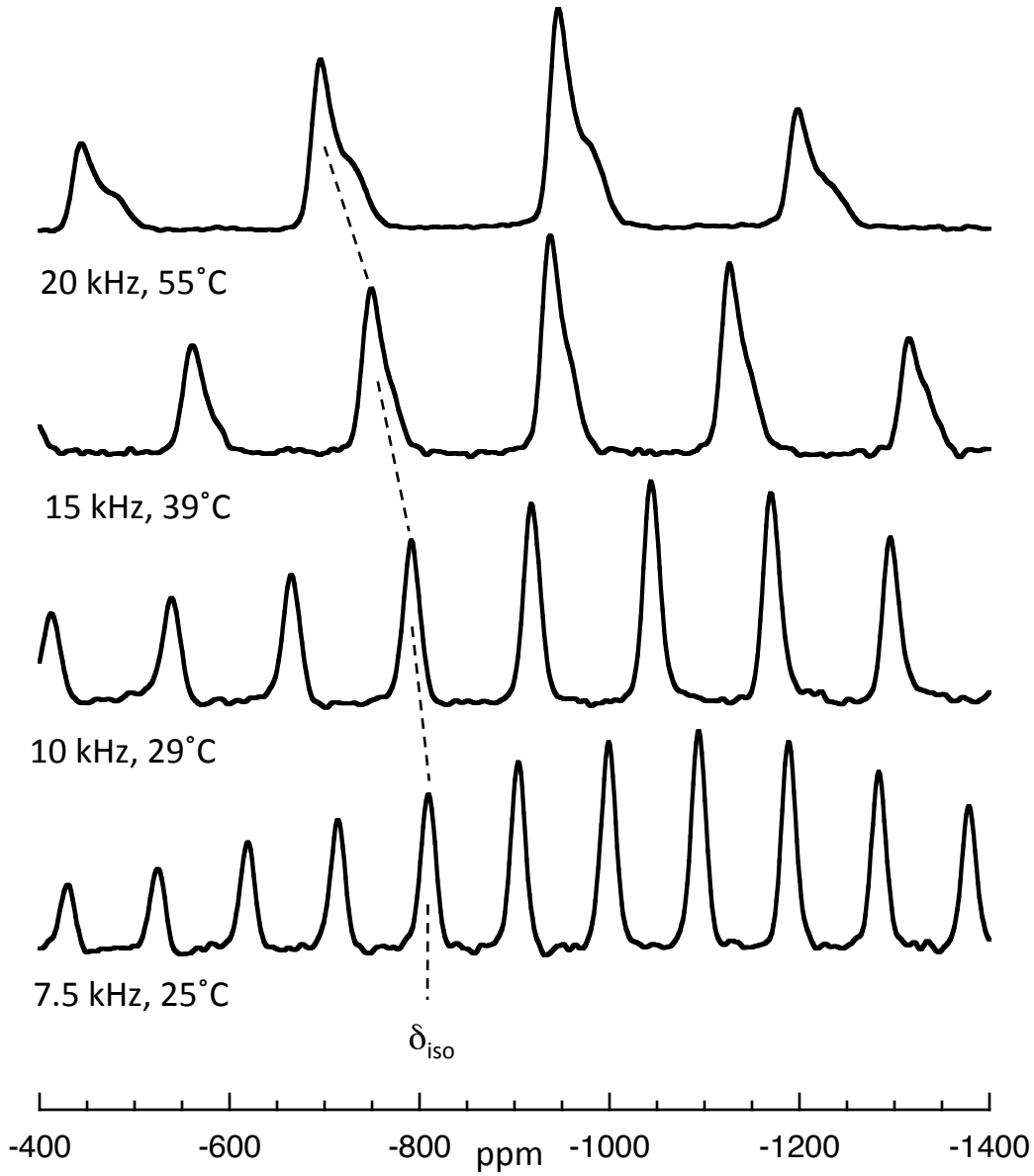
20 kHz, 55˚C
15 kHz, 39˚C
10 kHz, 29˚C
7.5 kHz, 25˚C
δiso
-400
-600
-800
ppm
-1000
-1200
-1400

Figure 4

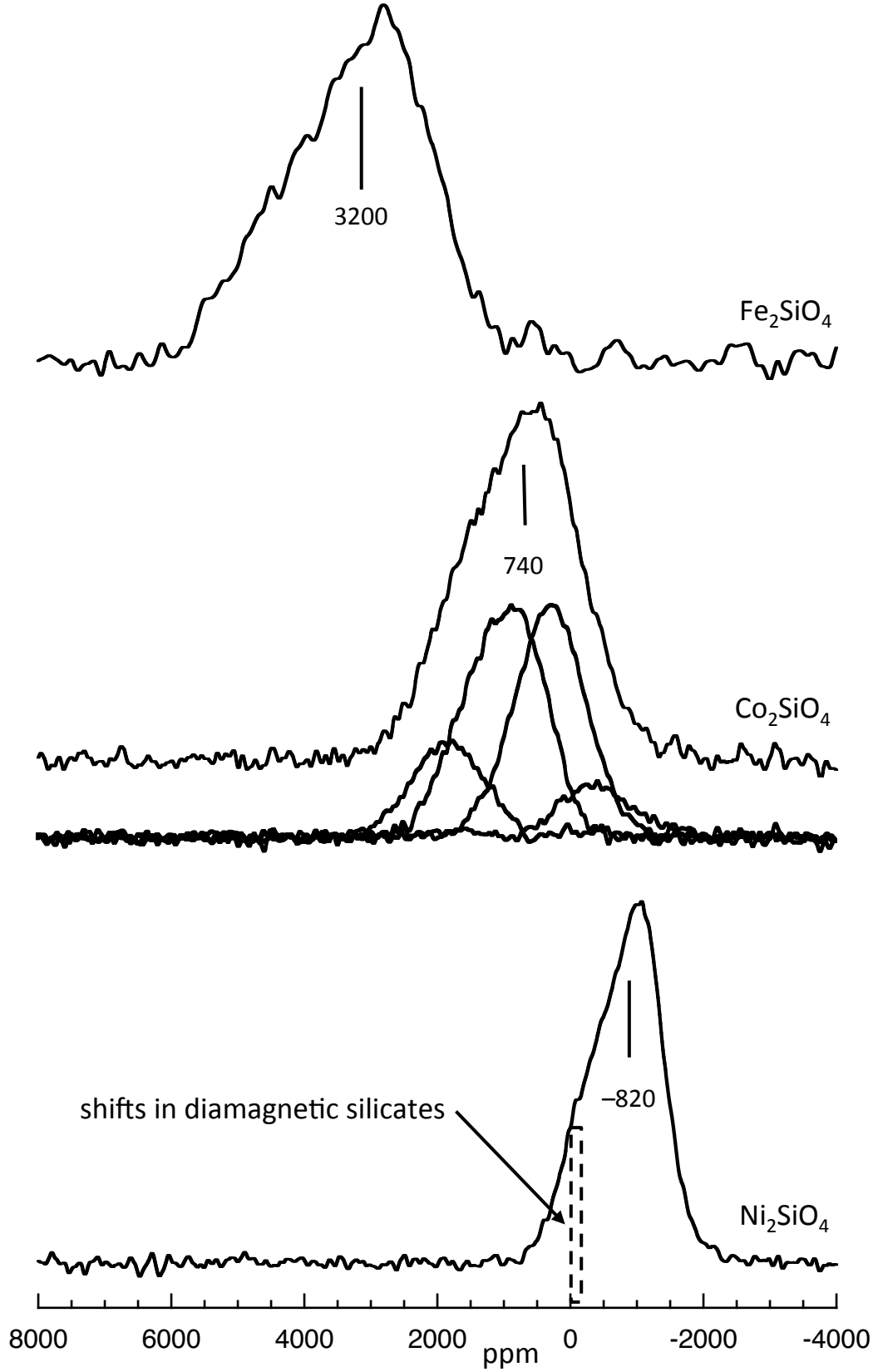
3200
Fe_2SiO_4
740
Co_2SiO_4
shifts in diamagnetic silicates
–820
Ni_2SiO_4
8000
6000
4000
2000
ppm
0
-2000
-4000

Figure 5

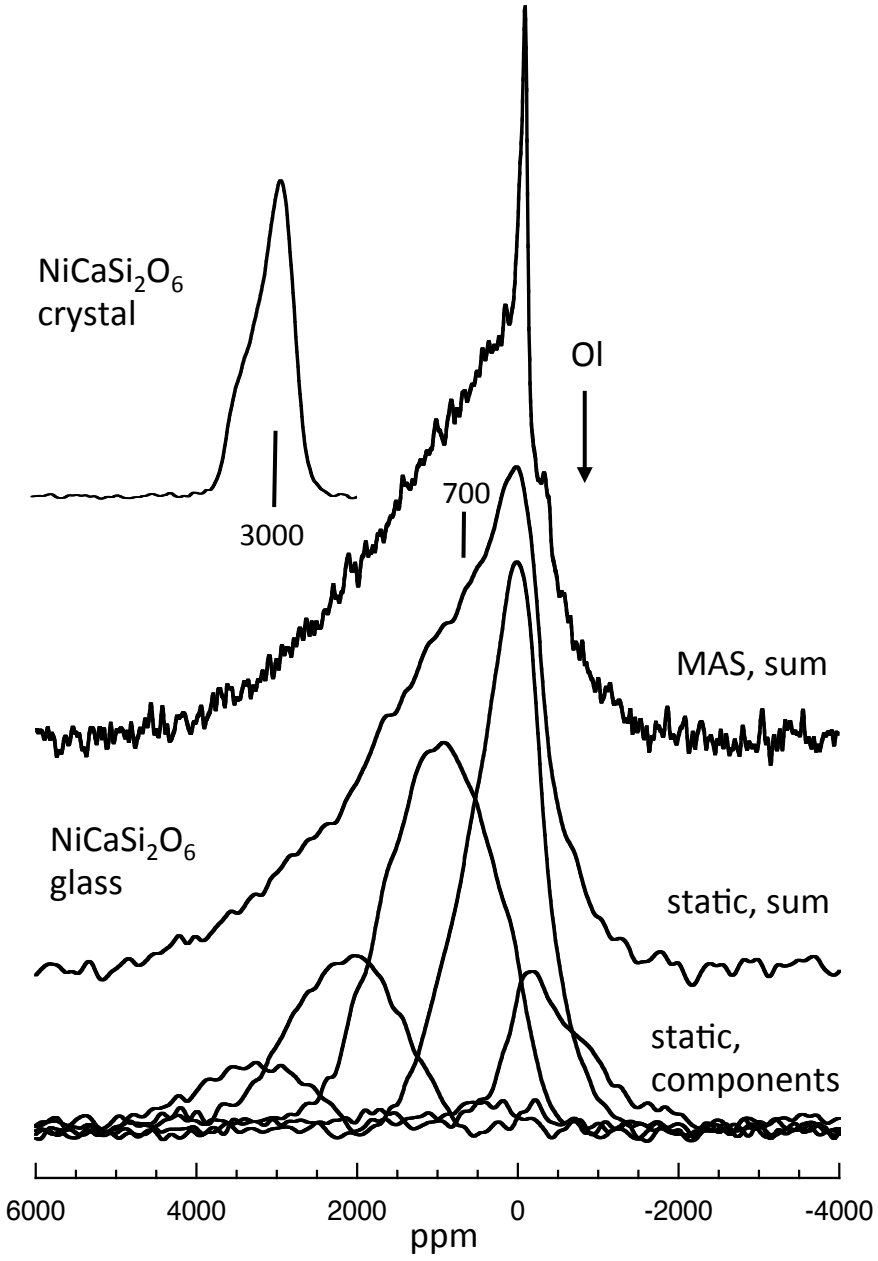
NiCaSi2O6
crystal
3000
Ol
700
MAS, sum
NiCaSi2O6
glass
static, sum
static,
components
6000
4000
2000
0
-2000
-4000
ppm

Figure 6

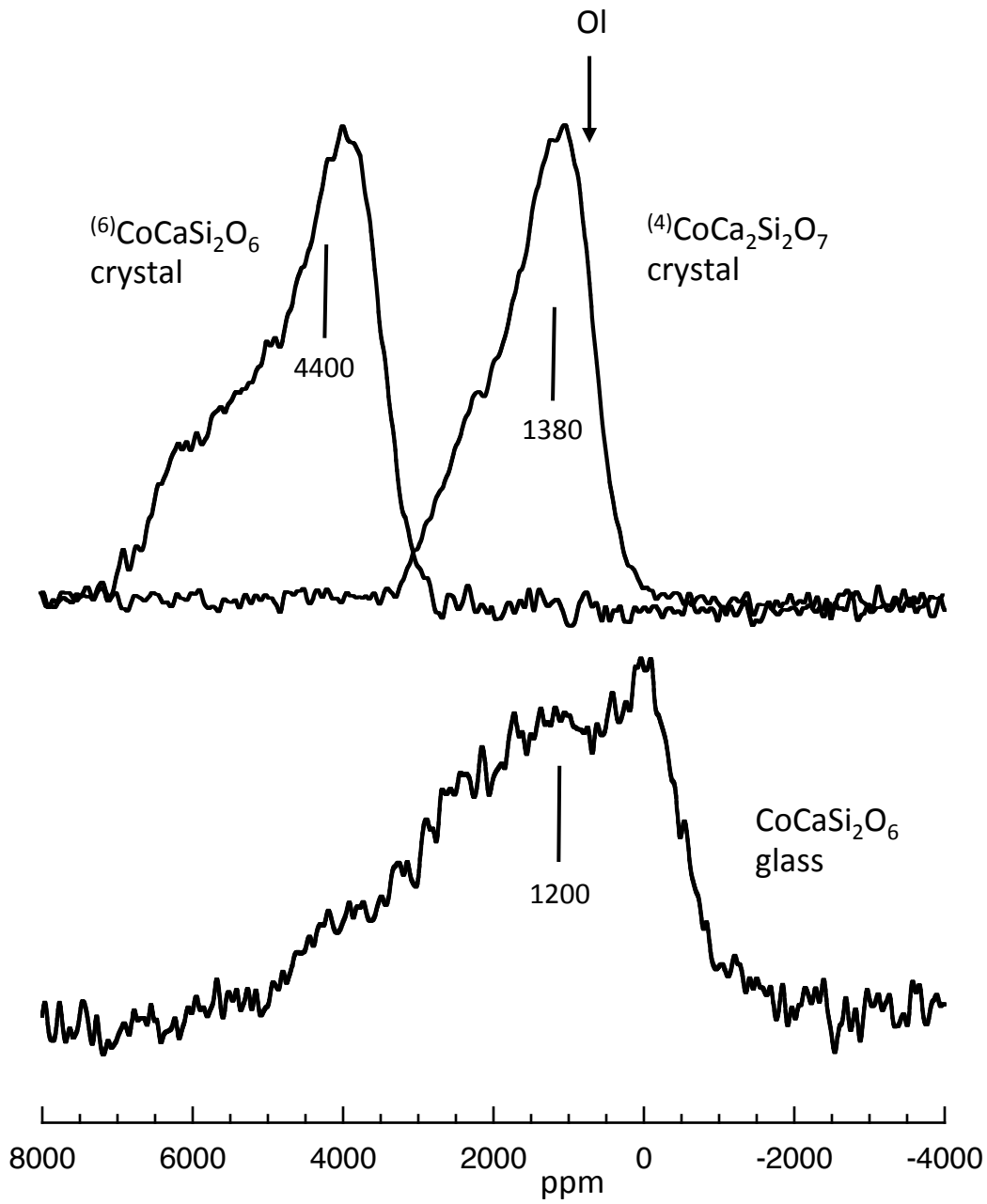
Ol
$^{(6)}CoCaSi_2O_6$
crystal
4400
$^{(4)}CoCa_2Si_2O_7$
crystal
1380
$CoCaSi_2O_6$
glass
1200
8000
6000
4000
2000
0
-2000
-4000
ppm

Figure 7

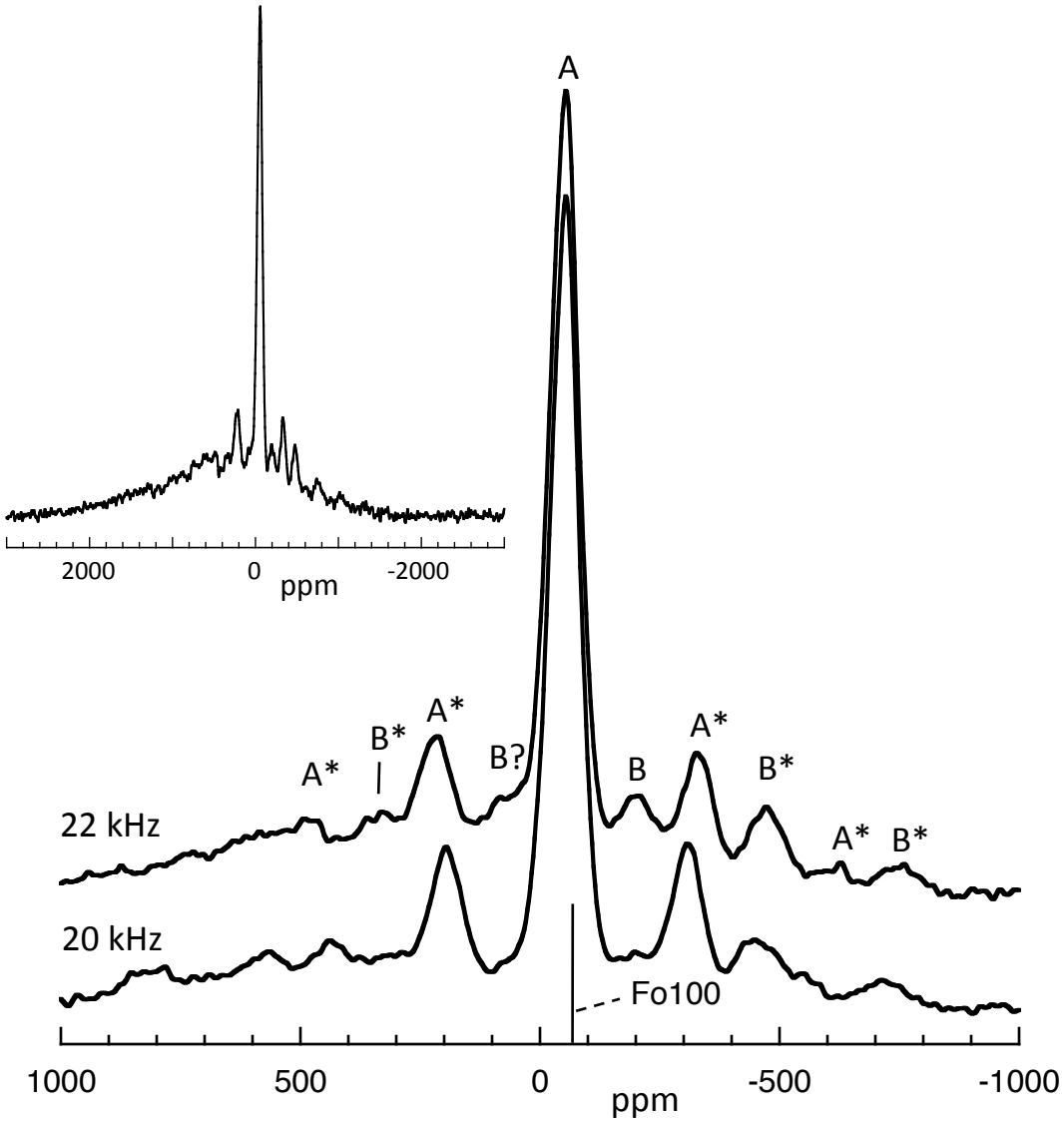
2000
0
-2000
ppm
A
A*
B*
A*
B?
B
A*
B*
A*
B*
22 kHz
20 kHz
Fo100
1000
500
0
-500
-1000
ppm

Figure 8

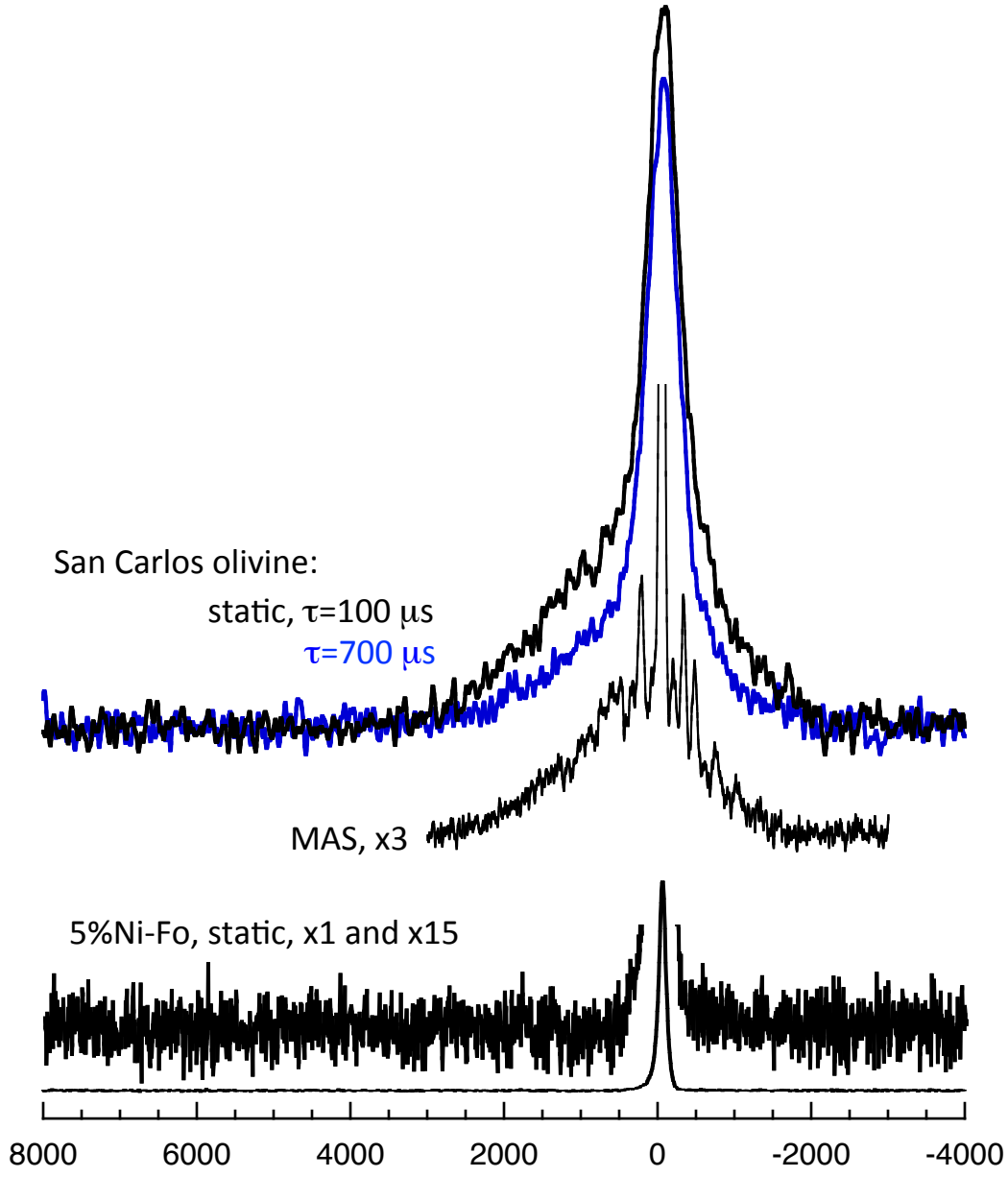
San Carlos olivine:
static, τ=100 μs
τ=700 μs
MAS, x3
5%Ni-Fo, static, x1 and x15
8000
6000
4000
2000
0
-2000
-4000

Figure 9

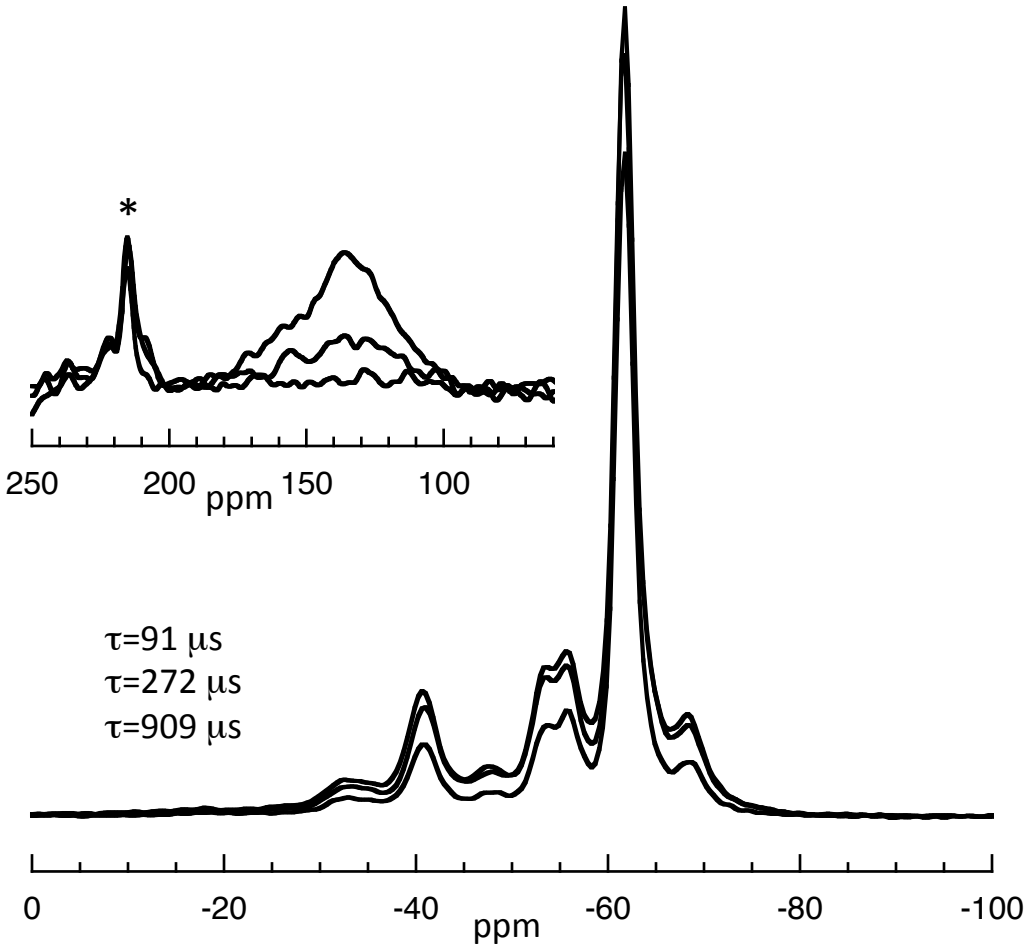

Figure 10

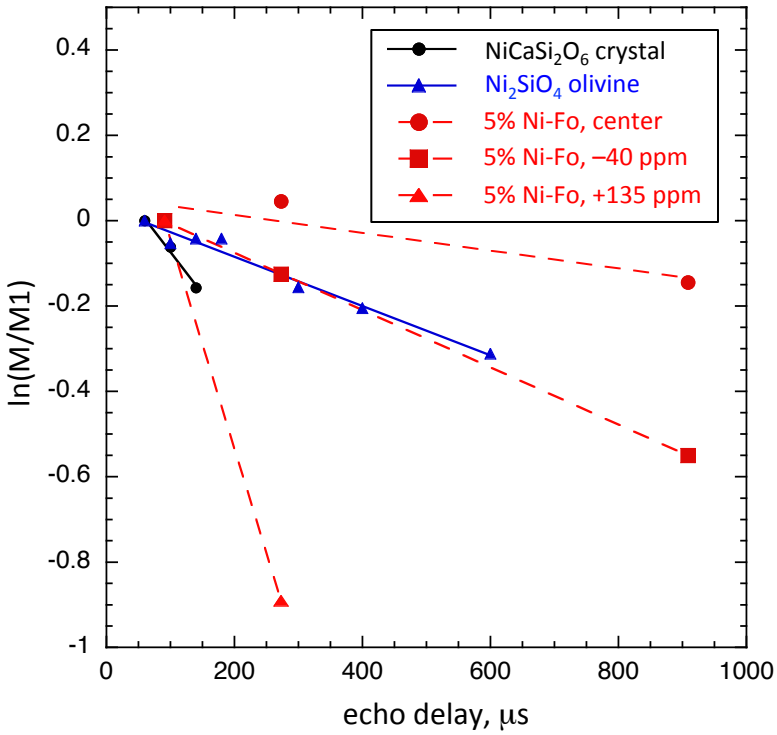
NiCaSi2O6 crystal
Ni2SiO4 olivine
5% Ni-Fo, center
5% Ni-Fo, –40 ppm
5% Ni-Fo, +135 ppm
ln(M/M1)
0.4
0.2
0
-0.2
-0.4
-0.6
-0.8
-1
0
200
400
600
800
1000
echo delay, μs

Figure 11

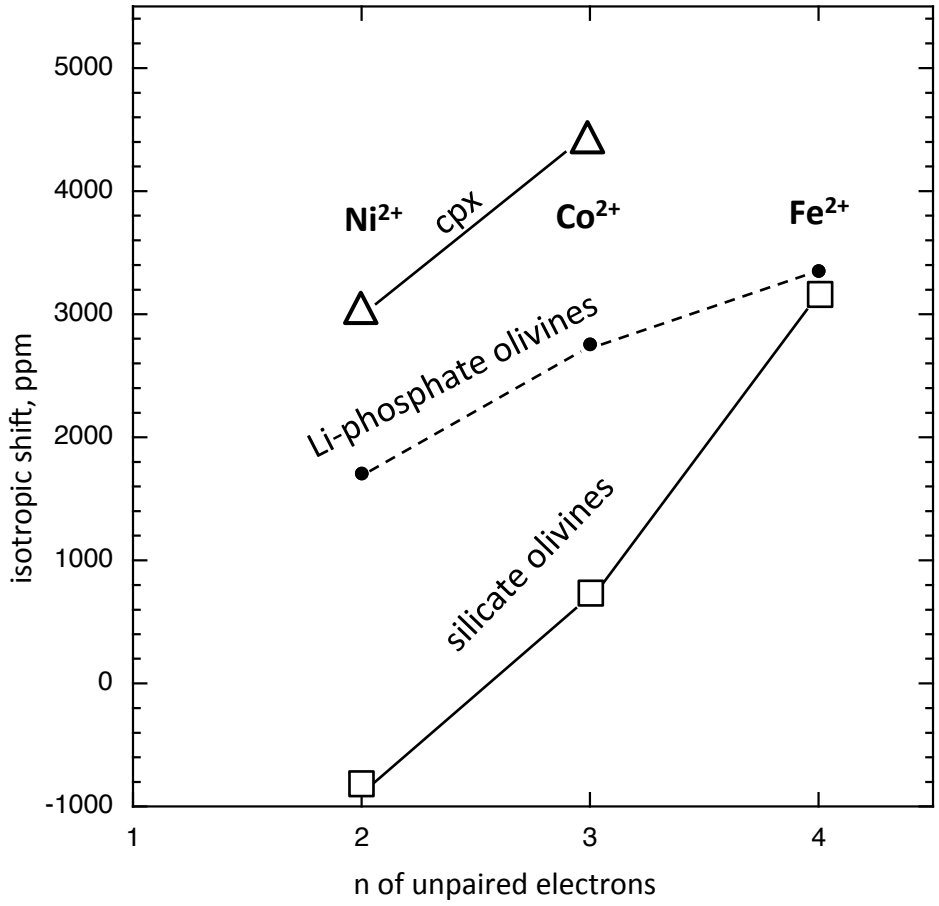
5000
4000
3000
2000
1000
0
-1000
isotropic shift, ppm
1
2
3
4
n of unpaired electrons
Ni2+
cpx
Co2+
Fe2+
Li-phosphate olivines
silicate olivines

Figure 12

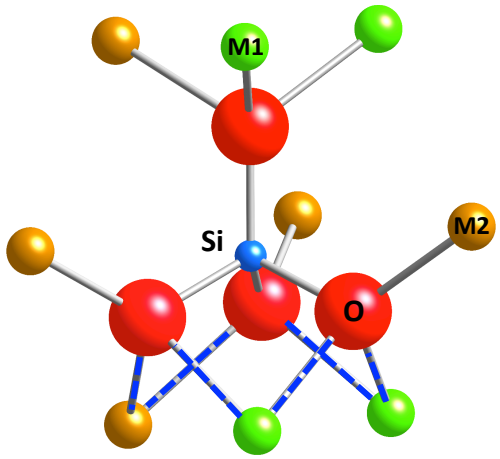

M_2SiO_4 olivine

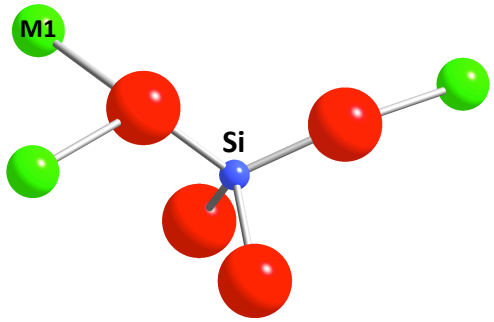

$MCaSi_2O_6$ clinopyroxene